CHARGE/DISCHARGE AND ELECTROMAGNETIC RADIATION STUDIES ON SPACECRAFT MATERIALS AND STRUCTURES

K. G. Balmain

Department of Electrical Engineering
University of Toronto

Toronto, Canada

FINAL REPORT

prepared for

THE DEPARTMENT OF COMMUNICATIONS, OTTAWA, CANADA

DSS Contract No. OSU76-00064

April 1977

CHARGE/DISCHARGE AND ELECTROMAGNETIC RADIATION STUDIES ON SPACECRAFT MATERIALS AND STRUCTURES

final report

K. G. BALMAIN

Department of Electrical Engineering

University of Toronto

Toronto, Canada

FINAL REPORT

prepared for

THE DEPARTMENT OF COMMUNICATIONS, OTTAWA, CANADA

DSS Contract No. 0SU76-00064

April 1977

TABLE OF CONTENTS

		Page
Acknowledgment		(i)
Personnel; Publication		(ii)
1.	Introduction	1
2.	Charge Imaging	6
3.	Micro-Discharges	27
4.	Macro-Discharges	32
5.	Electromagnetic Wave Attenuation in a Charged Dielectric	42
6.	Pulse Propagation on Complex Structures	47
7.	Conclusions and Recommendations	63
8.	References	67

ACKNOWLEDGMENTS

Thanks are expressed to Dr. M. Palfreyman (Scientific Authority for the contract) and to Dr. J. V. Gore for many helpful discussions and for providing the spacecraft materials used in the experiments. Thanks are also expressed to W. L. Lehn of the U.S. Air Force Materials Laboratory for providing a specimen of quartz fabric. The assistance of Dr. W. C. Nixon of Cambridge University is deeply appreciated.

PERSONNEL

K. G. Balmain, Professor. Principal Investigator.

P. C. Kremer, Electronics Technologist.

M. Cuchanski, Graduate Student.

J. N. Nkeng, Engineering Assistant.

P. A. Maasland, Undergraduate Student.

PUBLICATION

A paper entitled "Surface Microdischarges on Spacecraft Dielectrics", by K. G. Balmain, M. Cuchanski and P. C. Kremer has been submitted for the Proceedings of 1976 NASA/USAF Spacecraft Charging Technology Conference.

1. INTRODUCTION

K. G. Balmain

1.1 Background

Operational anomalies in the performance of synchronous-orbit spacecraft had started to receive special attention by 1970, and by 1972 the idea had become established that many of these anomalies might be caused by the magnetospheric environment. The overall electrostatic charging of a whole satellite is governed mainly by the balance between incident electron flux and photoemissive electron flux. Sudden increases in high-energy incident electron flux are associated with the onset of geomagnetic substorms, and these high energy electrons are most numerous in the midnight-to-dawn sector (local time). The most pronounced decrease in photoemission is associated with eclipse conditions, as the spacecraft passes into the earth's shadow. The energetic-particle measurements of De Forest [1972] established the existence of whole-satellite charging by showing that the satellite potential had an "energy-filter" effect on the incident particle flux, and that dramatic changes in this effect were associated with substorm and eclipse conditions. At about the same time laboratory experiments involving high-voltage, capacitor-like configurations were developed by Fredricks and Scarf [1973], motivated by the observation that severe spacecraft operational anomalies were associated with substorm and eclipse conditions. Laboratory experiments on electron beam charging of open surfaces of spacecraft dielectrics were carried out in a scanning electron microscope (SEM) by Balmain [1973] who noted complex patterns of charge accumulation and retention together with occasional apparent discharges involving electron emission. Subsequent developments

in this field of study do not need to be reviewed here because they have been thoroughly surveyed in the literature [Rosen 1975, 1976a, 1976b, 1976c].

Some worthwhile historical points do not emerge readily from a study of the literature, however. Consider for example the far-reaching influence of a small meeting of interested researchers held at the U.S. Space and Missiles Systems Organization in Los Angeles in November 1974. At this meeting there arose the idea of charge "cleanoff" of a large area of dielectric surface in the course of a discharge event. Another point is that up to the time of this meeting, differential charging had become established as the energy storage mechanism for destructive discharges, but differential charging had been associated only with capacitor-like sandwich configurations of spacecraft materials or with charge density variations tangentially across the surface of a charged dielectric. At the meeting Meulenberg advanced the idea of charge variation with depth in the dielectric as a cause for normally directed discharges, an idea that has become widely accepted [Meulenberg, 1976].

The most comprehensive existing collection of papers on the subject of spacecraft charging is in the book edited by Rosen [1976 b]. In it, extensive laboratory tests of large specimens are reported [Hoffmaster and Sellen,1976; Stevens, Lovell and Gore, 1976] and experimental evidence for charge cleanoff is presented in the foregoing and other papers [Adamo and Nanevicz, 1976; Balmain, Orszag and Kremer, 1976]. These papers taken together show that electrons with energies over a few keV, when incident on a metal-backed dielectric surface,

produce electrostatic charging and eventual physically-damaging arc discharges in which currents of the order of 100 A to 1000 A could flow for a few hundred nanoseconds into the metal backing on spacecraft-size specimens. This current flow must of necessity be accompanied by an equal current of electrons ejected outward into space.

1.2 Relation to Other Scientific Disciplines

Charge accumulation and decay in dielectric materials is the central issue in the study of electrets for use in condenser microphones. Some fluorocarbon electrets have estimated embedded-charge lifetimes of tens to hundreds of years at room temperature [Reedyk, 1968; Sessler and West, 1968]. These lifetimes have been estimated by observations on accelerated decay at elevated temperatures. These techniques have been refined to produce thermal "spectra" of thermally stimulated discharge currents during the decay of surface charge on polymer electrets [Creswell, Perlman and Kabayama, 1972; Van Turnhout, 1975].

Most electrets are made by heating and then cooling a dielectric material in a strong electric field. Electron beams have also been employed to form electrets [Sessler and West, 1970; Gross, Sessler and West, 1973] but the research papers do not mention spontaneous discharges. This is curious because if (according to the Meulenberg theory) the voltage between the embedded-electron layer and the exposed surface is of the order of the beam accelerating voltage, this would mean 20 kV over 10 μm, or two to three times the breakdown

field of typical polymers [O'Dwyer, 1973]. At very high energies the situation is not greatly different, considering that a 2 MeV beam of electrons did not produce spontaneous discharges in borosilicate glass or plexiglas [Gross, 1957; Gross, 1958] although a grounded needle probe was sufficient to initiate a strong discharge which caused a feather pattern of permanent damage at the penetration depth of the electrons. It is not clear why spontaneous discharges sometimes occur and sometimes do not. However the two factors of long charge lifetime and susceptibility to a very small stimulation both combine to suggest that in synchronous orbit a dielectric surface discharge could occur long after the spacecraft encountered energetic electrons.

Clearly a solution to the problem would be the development of conducting polymers with suitable thermal, infra-red, ultra-violet and mechanical properties. Development of such materials still could be years into the future. Such development would have to relate to the field of organic semiconducting polymers [Katon, 1968], a field which appears to be at a relatively primitive stage in its evolution.

1.3 Facilities at the University of Toronto

For the sake of convenience, economy and flexibility, the approach taken at the University of Toronto has been to utilize existing scanning electron microscopes for tests on spacecraft dielectrics. Two such SEMs have been used so far, namely a Cambridge S-4 standard SEM and a Science Data Technology (SDT) television-type SEM. A Coates and Welter field-emission SEM is also available but has not yet been used.

The Cambridge and the SDT SEMs do not have liquid nitrogen traps in their vacuum systems, so the possibility of diffusion pump oil (silicone type) backstreaming into the specimen chamber must be considered. If the discharge phenomenon under study were entirely a subsurface phenomenon, then a small degree of contamination in the specimen chamber would not be critical, because the main purpose of the vacuum would be to allow the electron beam access to the specimen. However it must be remembered that beam-induced conductivity in some sense "connects" the interior of the specimen to its surface, so that a high level of surface contamination must have some effect and should be avoided.

2. CHARGE IMAGING

M. Cuchanski

Irradiation of a dielectric material by a low energy (1-30 keV), low current density (~10 nA/cm^2) stream of electrons produces a layer of charge on, and just below, the surface of the dielectric. We tried a variety of experimental techniques to study the properties of the charged layer. Of these, the most fruitful proved to be the use of a unique feature of a SEM - its ability to "see" charge. Other methods were used in conjunction with the SEM studies and played a secondary role. Looking for signs of mechanical damage caused by micro-discharges (of which we found none) we employed a high power optical microscope. A different attempt at making the surface charge distribution visible with optical means was made utilising polarized light. A thin transparent, or translucent, charged dielectric sheet was inserted between two cross-polarized filters and examined in transmitted light. However, the anisotropy caused by the charge-induced stress in the sheet is apparently too small to produce a detectable rotation of the direction of polarization. Another method involved measurements of the electric field near the dielectric surface, done with a coaxial probe and a Keithley electrometer, these results confirming the images obtained with the SEM. And finally, we tried the old technique of sprinkling the charged surface with a fine mixture of powdered lead oxide and sulphur. This technique works very well when charges are deposited on the dielectric by DC discharges occurring in air or in a soft vacuum, yielding the classical Lichtenberg figures of breakdown streamers, but so far it has failed to map out the

charge patterns on surfaces irradiated in the relatively hard vacuum of the SEM. Either the presence of a sufficient number of ions is necessary for the technique to work successfully (the ions cling to the surface along a discharge path and attract differentially-charged powder particles), or further improvements in experimental technique must be made.

In a SEM the specimen surface is scanned with a focused electron beam in a square raster. The beam ionizes by impact the atoms in the upper layers at the point of incidence and ejects a cone of secondary electrons. The secondary electrons are collected and the signal thus obtained is used to modulate the intensity of an oscilloscope beam; the beam scans the oscilloscope screen in synchronism with the main raster. The source of image contrast is the variation in the number of collected electrons (secondary-electron emission yield) as the beam travels across the surface. The variation is due primarily to changes in the topography and the chemical composition of the specimen surface. Here, however, we are interested in another cause of variation -- the presence of the electric field produced by a surface charge. If a layer of charge exists beneath the surface at the point of incidence, the repulsive forces between it and the secondary electrons will propel the electrons upwards and increase their chances of reaching and leaving the surface. Thus the collector signal increases and we observe a bright spot. In this manner even a deeply submerged charge distribution can be mapped out, especially if the incident beam has sufficiently low energy so that it cannot penetrate to the depth at which the charge is buried; otherwise the charge distribution would be disturbed by the beam. This is the reason why in what follows the charge deposition was done at beam energies of 20-30 keV, while for viewing a 1 keV beam was used.

For a given material the secondary electron emission depends on the energy of the incident beam. The relation between the two takes the form of a secondary emission curve, such as shown in Fig. 2-1, where the ratio of the number N_s of emitted secondary electrons to the number N_i of incident electrons is plotted against the effective energy of the incident beam.

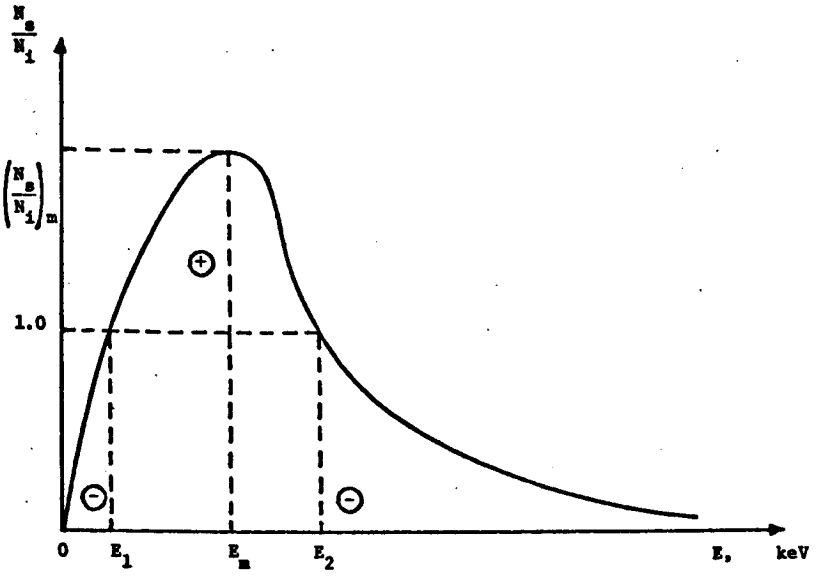

Fig. 2-1 Secondary electron emission curve

In the range of the incident beam energy for which $N_s/N_i > 1$, the specimen surface charges positively, while when $N_s/N_i < 1$, the specimen charges negatively. The values of E_1 and E_2 for polymers are quite low, for example for Teflon E_1= 0.05 keV, E_2 = 1.85 keV, the maximum yield occurring at E_m = 0.30 keV and being equal to 3.0; the corresponding values of Mylar are E_1= 0.02 keV, E_2 = 0.85 keV, E_m= 0.175 keV, $\left(N_s/N_i\right)_m$ = 4.8, and for Kapton E_1 = 0.03 keV, E_2= 0.5 keV, E_m= 0.15 keV, $\left(N_s/N_i\right)_m$ = 2.1 [Willis & Skinner, 1973]. The main point to be noted here is that beam energies of the order of 20 keV produce strong

negative charging of the polymers, while a 1 keV beam causes relatively weak charging, positive for Teflon and negative for Kapton and Mylar. Again we can see the advantage of using a low energy beam for the imaging of a surface charge distribution.

Depending on its energy and on the previous history of the irradiated dielectric, an incident beam can interact with the dielectric in several ways. It can deposit a charge on the surface, or, if the charge had been deposited there previously, it can clean it off. Since at a beam energy of 20 keV the depth to which the incident electrons can penetrate in polymers is about 10 μm, the beam can inject charge beneath the surface. Because of the very high intrinsic resistivity of these materials, the electrons are trapped there, and a charge build-up occurs. On the other hand, the beam-induced conductivity can be exploited to drain off the submerged space charge. The evidence for these phenomena is presented in the accompanying SEM micrographs.

When a flat dielectric surface is scanned by an electron beam in a dense raster, one is inclined to expect that the resulting charge distribution will be uniform. It turns out, however, that the actual charge distribution is highly nonuniform, as shown in the first micrograph of Fig. 2-2. The bright areas are strongly charged. This uneven distribution of charge on a homogeneous surface arises because of small differences in the secondary emission which always exist on adjacent portions of the surface; these initially small differences become accentuated during the process of charging as a nonuniform decelerating field builds up over the surface and changes the effective energy of the

(a) Teflon; charged at 20 kV by scanning beam, viewed at 20 kV, magnification 20X.	(b) Teflon; grid traced at 20 kV, viewed at 1 kV, magnification 20X.	(c) Protective Mylar on Silvered Teflon; grid traced at 20 kV, viewed at 1 kV, magnification 20X.
(d) Mylar; grid traced at 20kV, viewed at 1 kV, magnification 20X.	(e) Kapton; grid traced at 20 kV, viewed at 1 kV, magnification 20X.	(f) Quartz fabric; grid traced at 20 kV, viewed at 1 kV, magnification 20X.
(g) Teflon; grid node, surface charge removed to expose submerged charge, viewed at 1 kV, magnification 100X.	(h) Teflon; migration of charge along scratches on surface, viewed at 1 kV, magnification 100X.	(i) Quartz fabric; charged at 20 kV, viewed at 20 kV, magnification 500X.
(j) Quartz fabricat 150°C; charged at 20 kV, square due to step-up in magnification, viewed at 1 kV, magnification 20X.		

Fig. 2-2 Charge imaging in scanning electron microscope In each case, except (a) and (i), the specimen was exposed to air between the steps involving charging and viewing.


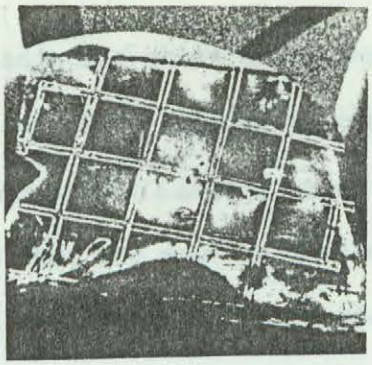
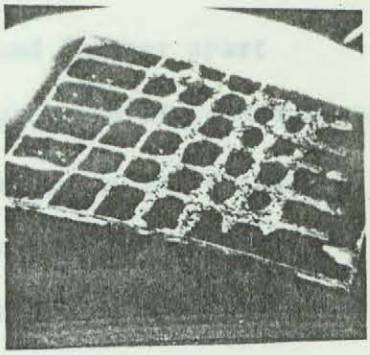
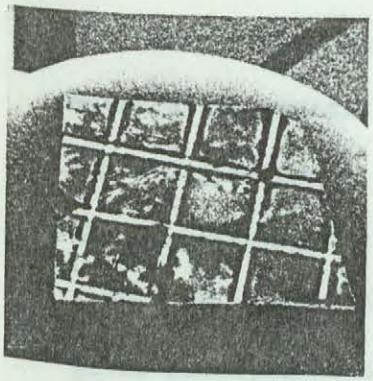
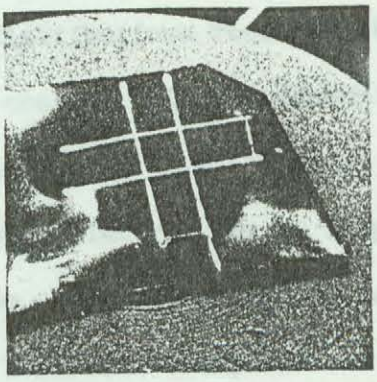
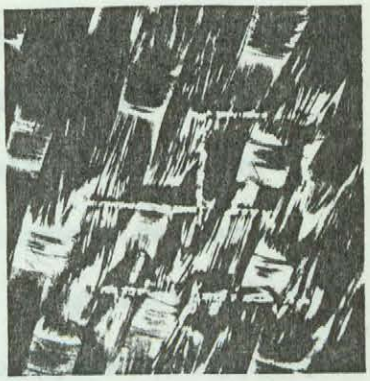
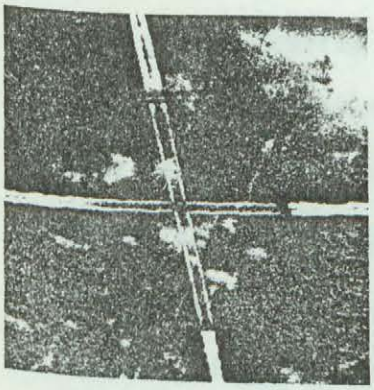
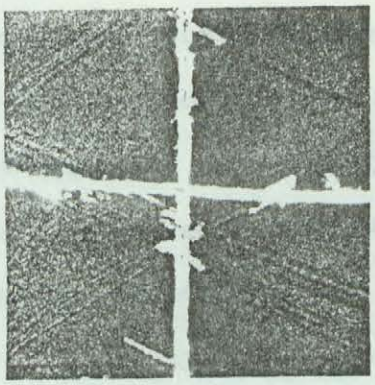

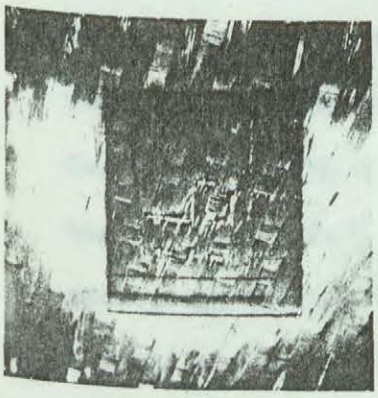

incident beam, and the adjacent areas drift farther and farther apart on the secondary emission curve. Electric stresses grow rapidly and may culminate in a disruptive surface discharge which redistributes the charge and partly restores equilibrium; the process then continues cyclically. It can be observed in real time or in a slow motion using a TV scan rate SEM, which is able to follow fast variations.

The surface charge distributions resulting from a raster scan are difficult to predict and control. In the Cambridge SEM a spot beam can be positioned and moved by the operator manually; this allows the experimenter to lay down electric charge in predetermined patterns. A grid of charge traced on a virgin surface is easily recognizable and gives excellent contrast between the exposed and the unexposed areas. The micrographs of Fig. 2-2 show grids deposited on several polymers and on a quartz fabric; the appearance of the pattern depends on the irradiated material. A characteristic feature of the grid is the double line structure best seen in the Teflon micrographs. The electric field over a line of charge forms a sharp "ridge" which wedges into the incoming beam and forces it apart; the electrons flow down on both sides of the ridge and are deposited at its base. The width of the base, initially equal to the beam diameter, becomes greater and greater as the charging process continues. This raises the important question of the effective irradiated area, which will be discussed shortly. Another interesting question is: are we dealing here with a surface charge only, or are the double lines buried beneath the surface of the dielectric? The answer can be seen in the micrograph of Fig. 2-2(g). Here a node of the grid had been bombarded for several minutes by 1 keV electrons in a square raster at a stepped-up

magnification. The bombardment removed the surface charge within the square and revealed the underlying, more permanent, submerged charge pattern. The surface charge can also be neutralized by exposure to air, but this does not provide such a convincing demonstration that what we are seeing is in fact a charge beneath the surface.

The charge patterns have long lifetimes at room temperature: the micrographs (b) and (d) in Fig. 2-2 were taken a week after the grid had been laid down; no dimming of the grid lines could be detected. The lifetime depends on the material and appears to be the longest for Teflon and Mylar; for some Kapton samples and in the case of the quartz fabric the grid disappeared after only a day or two. Besides the intrinsic properties of the material, other factors as well may determine the charge retention, the smoothness of the surface and the presence of contaminants being perhaps the most influential.

When the irradiated surface is not flat, charge tends to accumulate and migrate along edges. By way of illustration, a scratched Teflon sample is shown in Fig. 2-2(h). Streaks of charge which apparently migrated along scratches away from the grid lines are clearly seen. As for quartz fabric, the charging of individual strands is shown in the next micrograph.

The quartz fabric exhibited unusual charging behaviour. In the process of examining a dielectric material, an operator controlled step-up in magnification can be seen in a SEM as a bright or dark square (depending on the position on the secondary emission curve) on the background of the specimen surface. For Teflon, Mylar, and Kapton the square would

persist for a long time (minutes to weeks, increasing with the incident beam energy), a nuisance in most situations. In the case of the quartz fabric, however, the square would vanish in a few seconds. When the temperature of the sample was increased to 150°C, squares such as the one in Fig. 2-2 (j) were observed to persist for about a minute, certainly an unexpected result! Two explanations suggest themselves: either the charge retention ability of the quartz fabric increases with temperature, at least in this temperature interval (a local maximum), or its secondary emission yield is a sensitive function of temperature.

The effective irradiated area for a spot beam impinging upon a dielectric can be found by measuring the final width of the grid lines on the micrographs and dividing it by the magnification. An average of a number of measurements gives the final beam diameter as 80 μm, and consequently the effective area under a stationary or slowly travelling beam is 5.0×10^{-9} m^2. Thornton[1968] gives the spot size for a beam incident on a conducting specimen (the normal situation in a SEM) as 0.025 μm. The effect of charging is then a 32 hundred times increase in the beam diameter, or 10 million times increase in the irradiated area. The increase in the irradiated area does not cause, however, a corresponding decrease in the incremental charge density at the surface, since the incremental charge is concentrated in a narrow annulus (semi-annulus for a travelling beam); the annulus forms at the beginning of charging and then expands from the initial diameter of 0.025 μm to the final value of 80 μm.

The surface charge distribution on a dielectric near a grounded

conducting edge is another problem of interest in spacecraft applications. To study it, dielectric samples were coated with a thick layer of aluminium except for a central circular area, and the area was then irradiated with 20 keV electrons. The first micrograph in Fig. 2-3 shows a difficult-to-capture discharge event. It manifested itself during the photographic scan as a sudden jump in magnification. A discharge is accompanied by a collapse of the electric field over the sample surface; the field acts as an electrostatic lens, and its collapse causes the change in magnification. Both the first and the second of the micrographs of Figure 2-3, taken immediately after the irradiation, show an apparently uniform charge distribution. When, however, the surface charge was removed by exposing the sample to air, and the area was examined again, this time at 1 keV, a completely different picture emerged. As shown in the last micrograph of Fig. 2-3, the charge forms several concentric rings near the grounded edge. The particular area shown in Fig. 2-3 is 2.5 mm in diameter, but areas 5.0, 7.5 and 10.0 mm in diameter gave very similar results. Such a charge concentration must give rise to high tangential electric fields near the grounded edge; this was confirmed by electrometer measurements. The results indicate that venting holes in the thermal blanket material, and other dielectric-grounded conductor junctions on spacecraft structure, are under particularly severe electric stress.

The ability of a given material to store charge for an extended period of time can be estimated from its behaviour at elevated temperatures. A grid was laid down on a sample at room temperature using a 20 keV beam, the surface charge was removed by exposing the sample to air, and

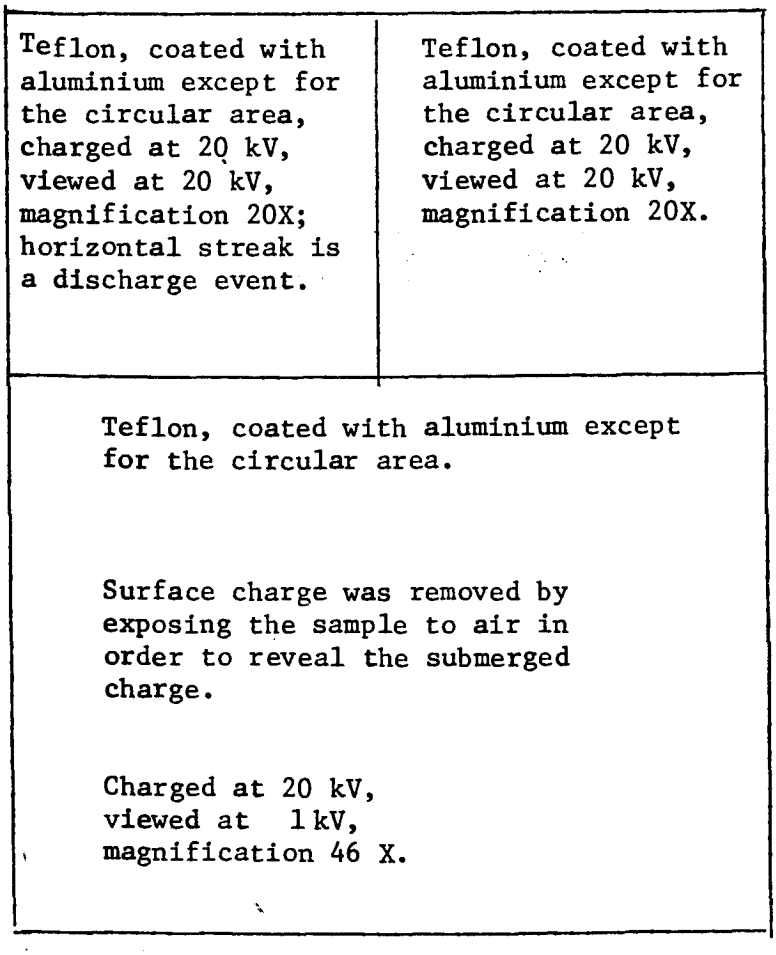

Fig. 2-3 Charge distribution on dielectric near grounded conducting edge.

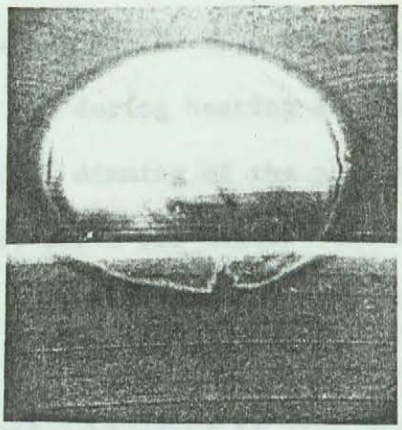

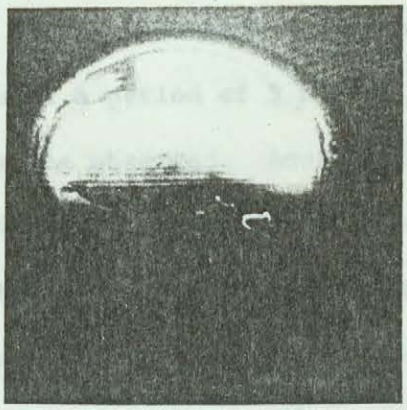

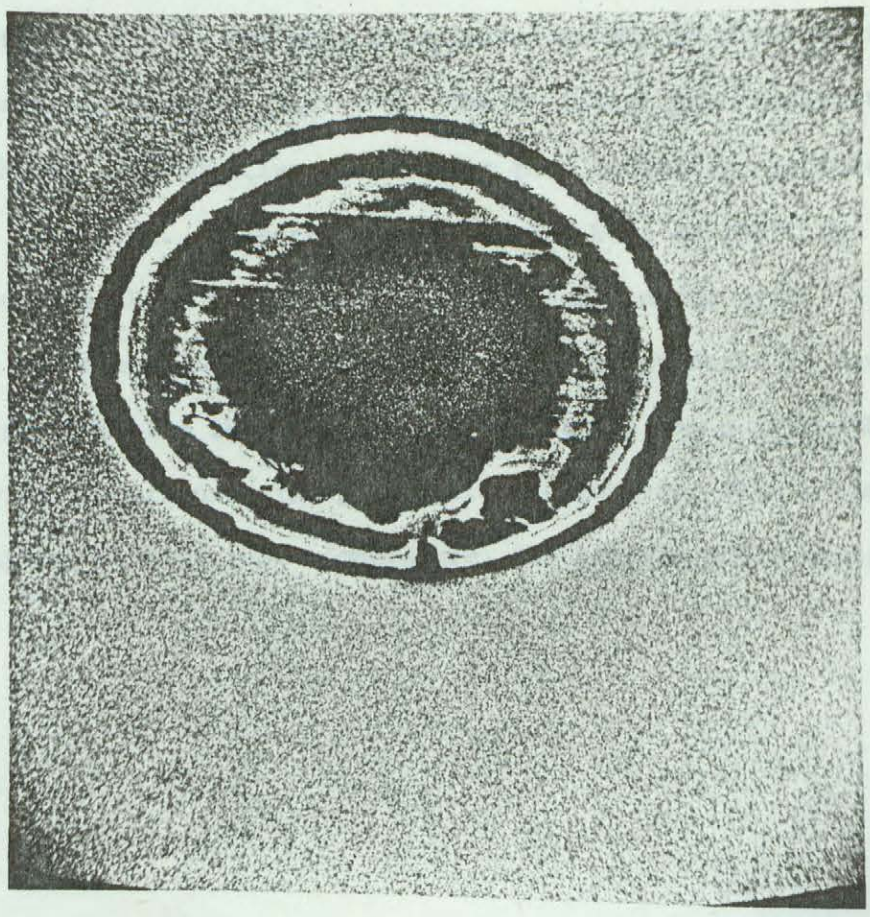

the embedded charge pattern was photographed at regular time intervals while the sample was kept at a constant elevated temperature. Thus it was found that Teflon demonstrates a very high charge retention even at temperatures above 100°C. The micrographs of Fig. 2-4 show a Teflon sample before and during heating at 115°C over a period of 5 hours. A small but gradual dimming of the pattern can be observed. Another Teflon sample, kept at 175°C for 1 hour and 20 minutes is shown in Fig. 2-5. Here the most prominent features are the streaks of charge diffusing away from the grid lines, probably along surface imperfections. Again a small but noticeable loss of line definition took place. When a Mylar sample was heated to 115°C, the grid disappeared within 30 minutes; the sequence of events is shown in Fig. 2-6. The diffusion time constant for charge in Mylar is evidently much shorter than in Teflon, indicating a lower charge retention. A quartz fabric sample, kept at 150°C for 2 hours 30 minutes, is shown in Figure 2-7. No change in the grid appearance can be detected. This is another piece of evidence in favour of the hypothesis that the charge retention ability of the quartz fabric may increase with temperature since, as mentioned earlier, when a sample of the material was kept at room temperature, the pattern would disappear rapidly.

Teflon sample, before grid deposition, viewed at 1 kV, magnification 20X, room temperature.	Grid deposited at 20 kV, sample exposed to air for a few seconds, viewed at 1kV, magnification 20X, room temperature.	Grid node, viewed at 1 kV, magnification 200X, room temperature. Heater switched on at this moment.
Grid node, viewed at 1 kV, magnification 200X after 30 min at 115°C.	Grid node, viewed at 1 kV, magnification 200X, after 1 h 10 min at 115°C.	Grid node, viewed at 1 kV, magnification 200X, after 1h 50 min at 115°C.
Grid node, viewed at 1 kV, magnification 200X, after 2 h 30 min at 115°C.	Grid node, viewed at 1 kV, magnification 200X after 3 h 10 min. at 115°C.	Grid node, viewed at 1 kV, magnification 200X, after 3 h 50 min at 115°C.
Grid node, viewed at 1 kV, magnification 200X, after 4 h 30 min at 115°C.	Grid node, viewed at 1 kV, magnification 200X, after 5 hours at 115°C.	The Teflon sample, viewed at 1 kV, magnification 200X, room temperature.

Fig. 2-4 Effect of temperature on charge retention in Teflon

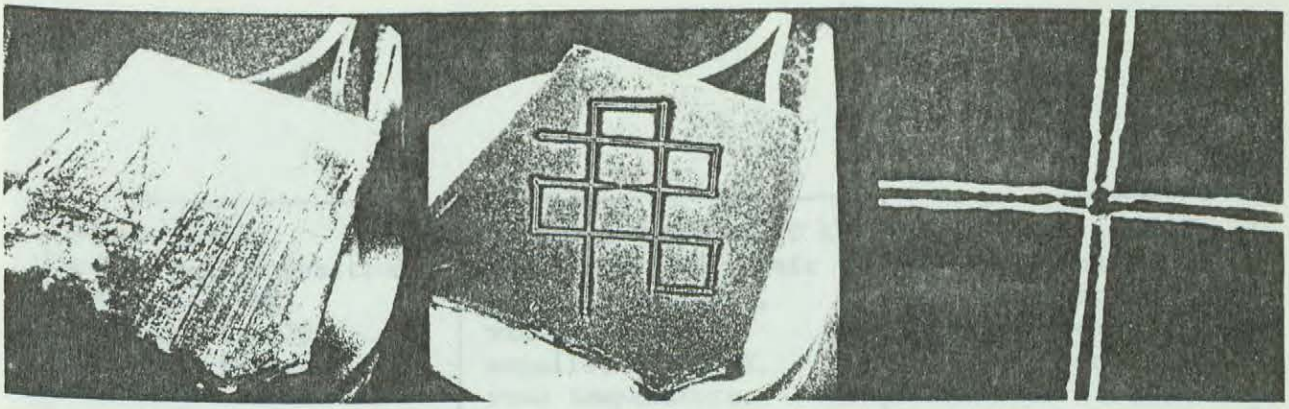

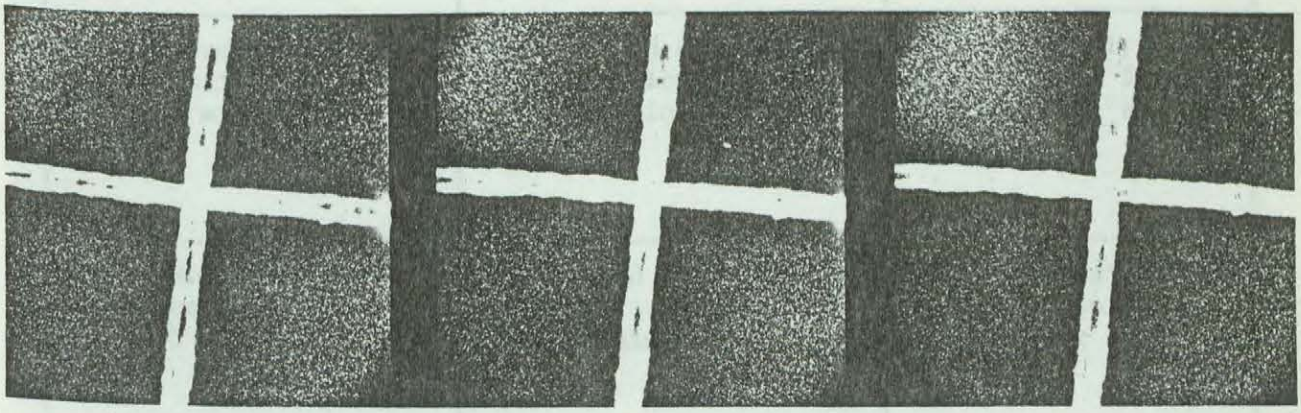

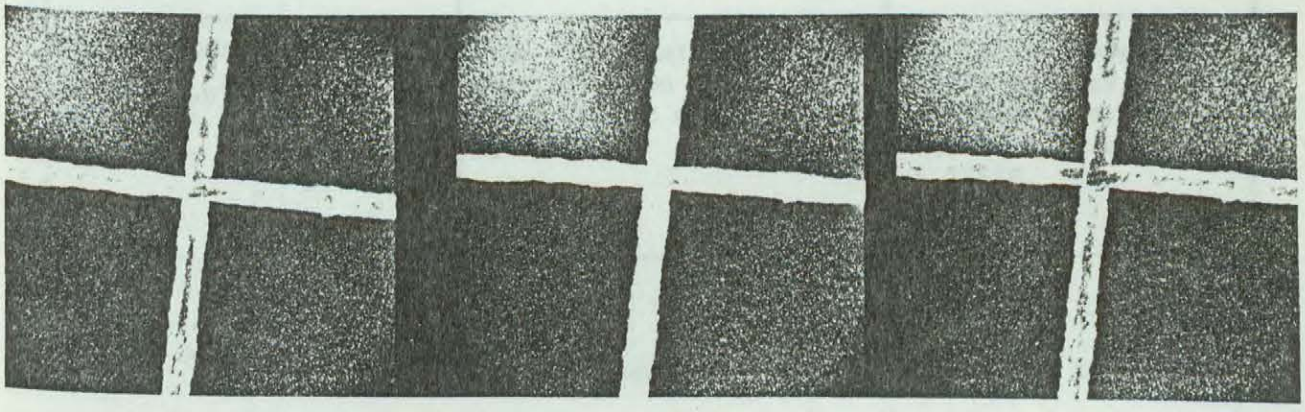

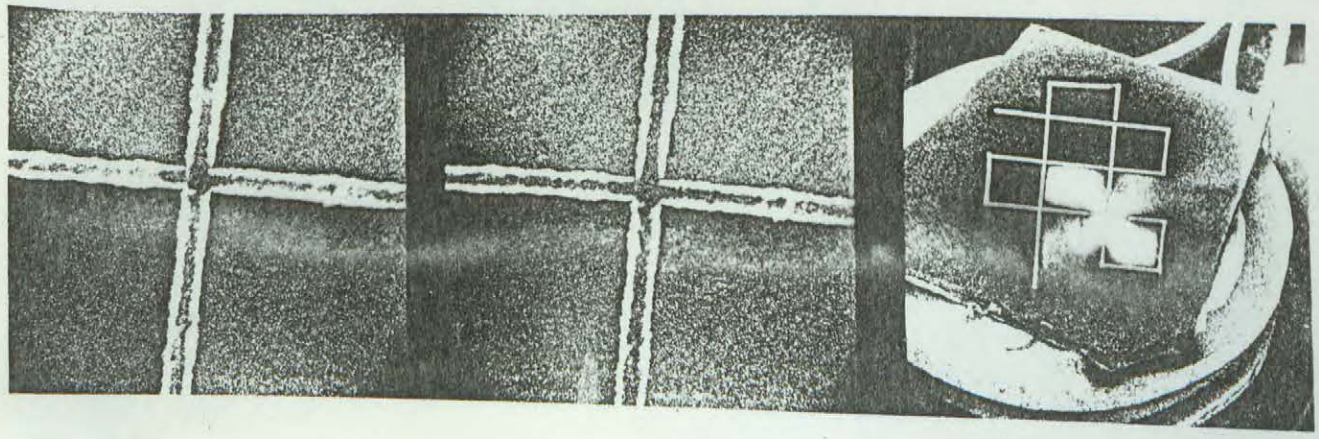

Teflon sample, before grid deposition, viewed at 1 kV, magnification 20X, room temperature.	Grid deposited at 20 kV, sample exposed to air for a few seconds, viewed at 1 kV, magnification 20X, room temperature.	Grid viewed at 1 kV, magnification 50X, room temperature. Heater switched on at this moment.
Grid viewed at 1 kV, magnification 50X, after 10 min at 175°C.	Grid viewed at 1 kV, magnification 50X, after 20 min at 175°C.	Grid viewed at 1 kV, magnification 50X, after 30 min at 175°C.
Grid viewed at 1 kV, magnification 50X, after 40 min at 175°C.	Grid viewed at 1 kV, magnification 50X, after 50 min at 175°C.	Grid viewed at 1 kV, magnification 50X, after 1 hour at 175°C.
Grid viewed at 1 kV, magnification 50X, after 1 h 10 min at 175°C.	Grid viewed at 1 kV, magnification 50X, after 1 h 20 min at 175°C	The Teflon sample, viewed at 1 kV, magnification 20X, after 1 h 20 min at 175°C.

Fig. 2-5 Effects of temperature on charge retention in Teflon.

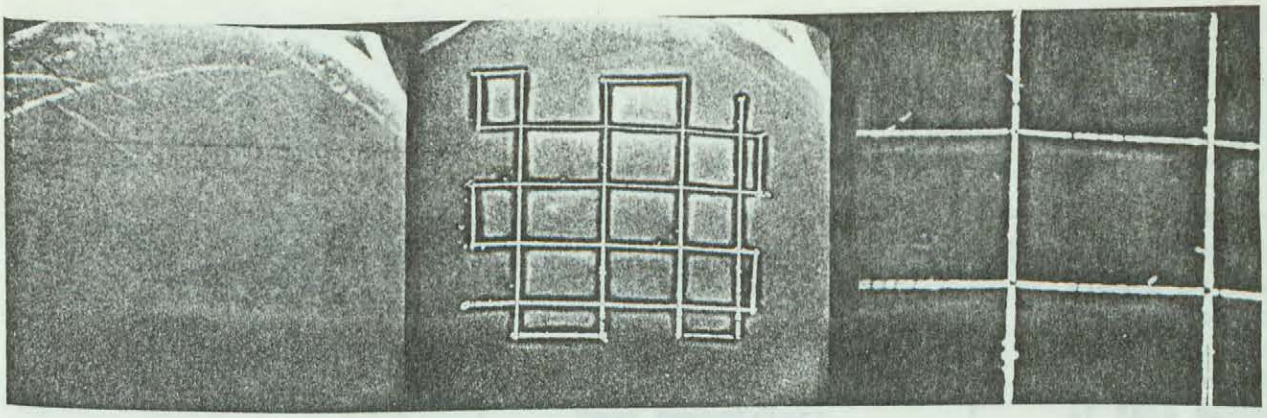

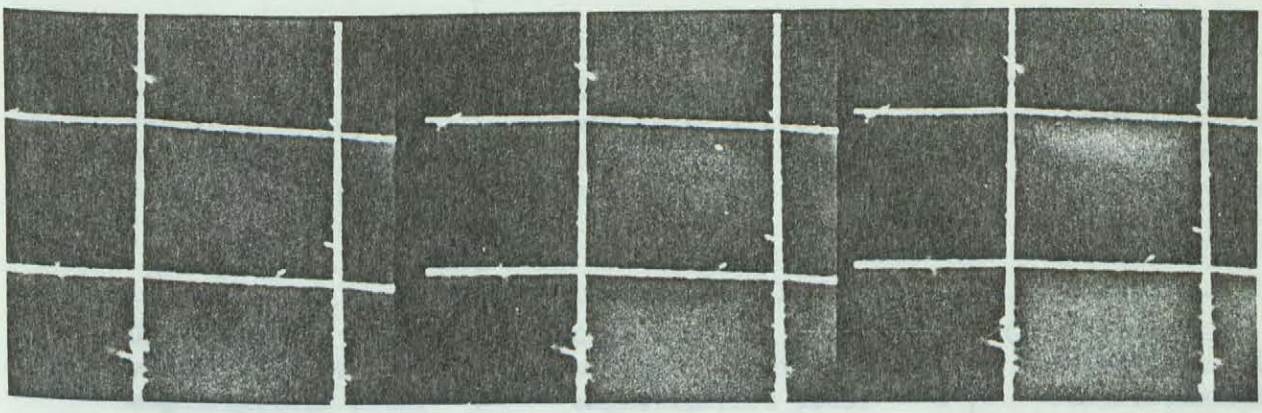

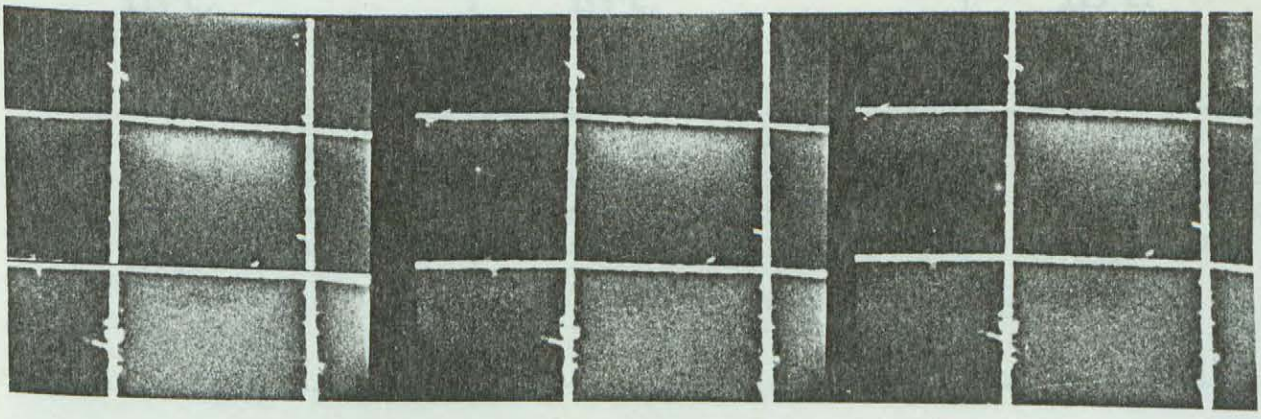

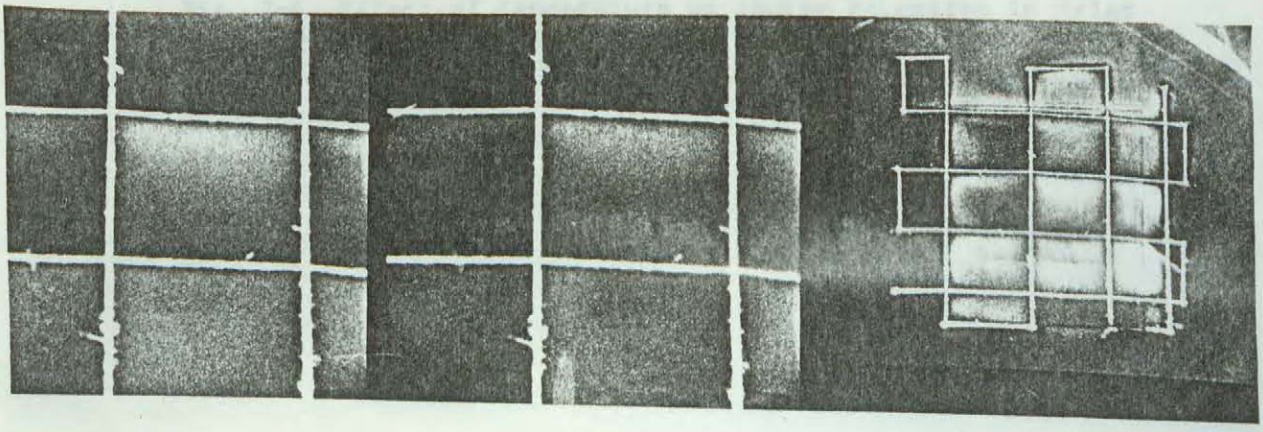

(a) Mylar sample, before grid deposition, viewed at 1 kV, magnification 20X, room temperature.	(b) Grid deposited at 20 kV, sample exposed to air for a few seconds, viewed at 1 kV, magnification 20X, room temperature.	(c) Grid node, viewed at 1 kV, magnification 200X, room temperature. Heater switched on at this moment.
(d) Grid node, viewed at 1 kV, magnification 200X, after 5 min at 115°C.	(e) Grid node, viewed at 1 kV, magnification 200X, after 8 min at 115°C.	(f) Grid node, viewed at 1 kV, magnification 200X, ater 11 min at 115°C.
(g) Grid node, viewed at 1 kV, magnification 200X, after 14 min at 115°C.	(h) Grid node, viewed at 1 kV, magnification 200X, after 17 min at 115°C.	(i) Grid node, viewed at 1 kV, magnification 200X, after 20 min at 115°C.
(j) The Mylar sample, viewed at 1 kV, magnification 20X, after 21 min at 115°C.	(k) The Mylar sample viewed at 1 kV, magnification 20X, after 25 min at 115°C.	(l) The Mylar sample, viewed at 1 kV, magnification 20X, after 30 min at 115°C.

Fig. 2-6 Effect of temperature on charge retention in Mylar

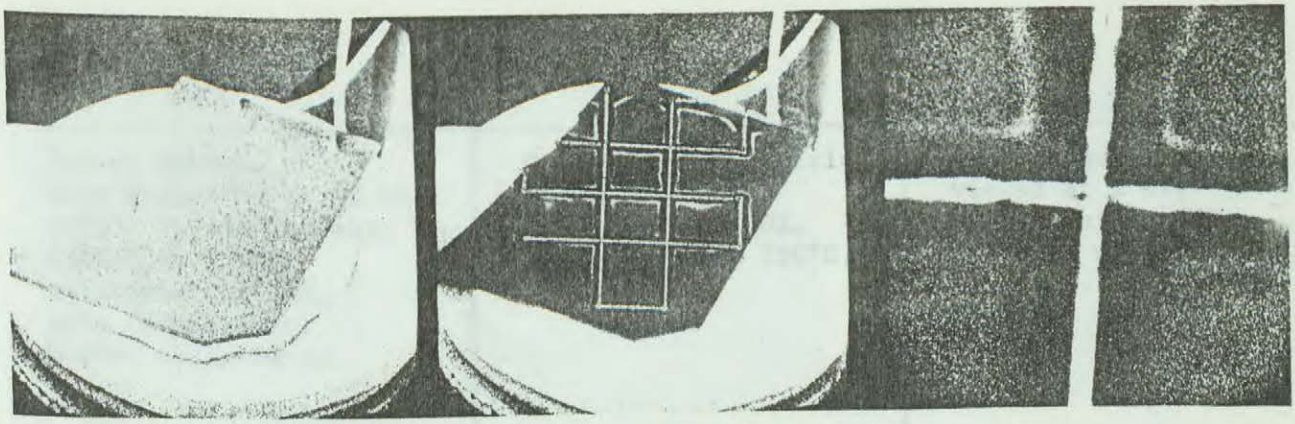

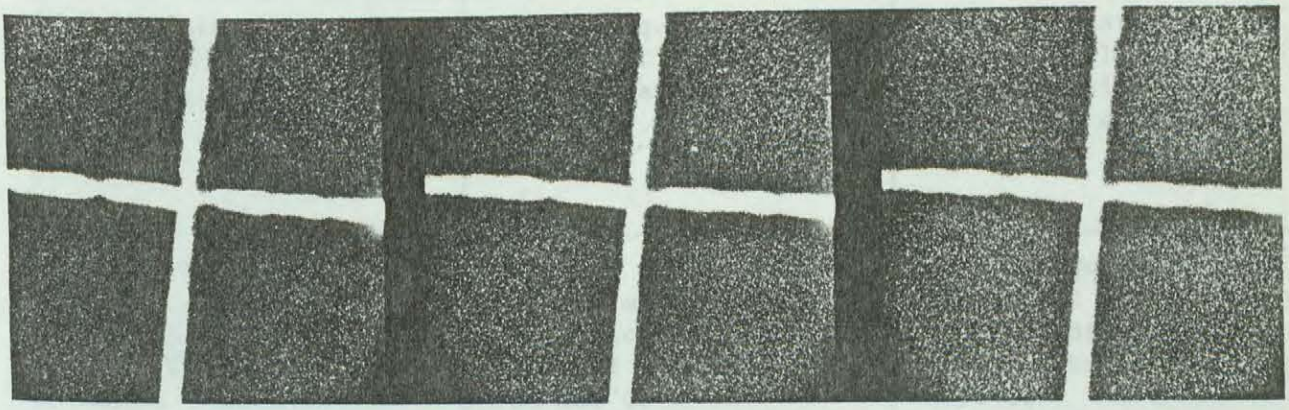

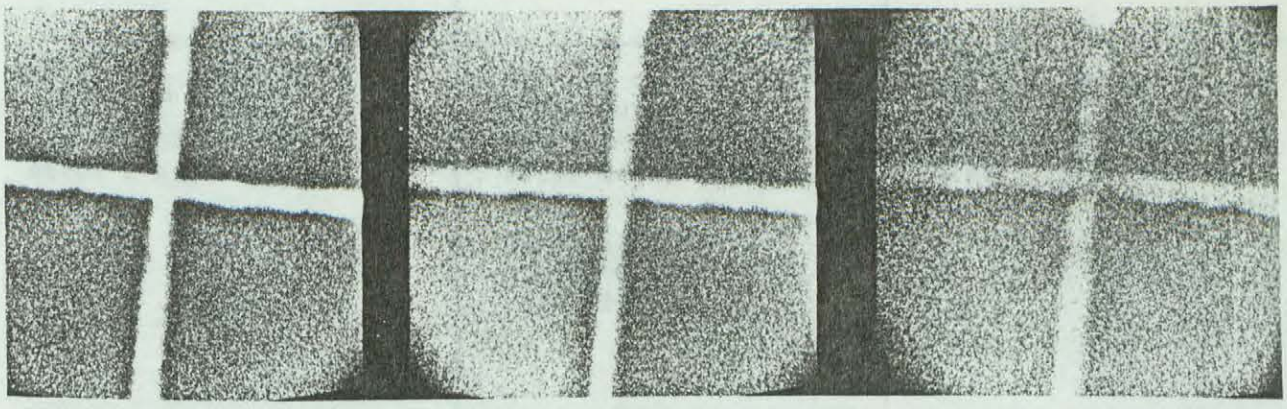

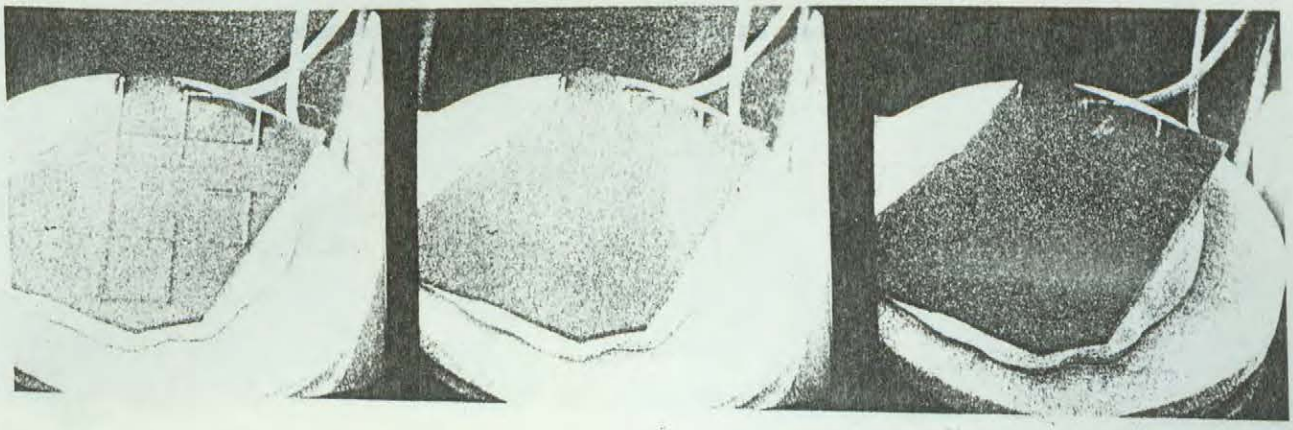

Quartz fabric, grid deposited at 20 kV, sample exposed to air, viewed at 1 kV, magnification 50X, room temperature. Heater switched on.	Grid on quartz fabric, viewed at 1 kV, magnification 50X, after 5 min at 150°C.	Grid on quartz fabric viewed at 1 kV, magnification 50X, after 10 min at 150°C.
Grid on quartz fabric, viewed at 1 kV, magnification 50X, after 20 min at 150°C.	Grid on quartz fabric viewed at 1 kV, magnification 50X, after 40 min at 150°C.	Grid on quartz fabric viewed at 1 kV, magnification 50X, after 1 h at 150°C
Grid on quartz fabric, viewed at 1 kV, magnification 50X, after 1 h 20 min at 150°C.	Grid on quartz fabric, viewed at 1 kV, magnification 50X, after 1 h 40 min at 150°C.	Grid on quartz fabric, viewed at 1 kV, magnification 50X, after 2 hours at 150°C.
Grid on quartz fabric, viewed at 1 kV, magnification 50X, after 2 h 20 min at 150°C.	Grid on quartz fabric, viewed at 1 kV, magnification 20X, after 2 h 30 min at 150°C. Dark square due to previous step-up in magnification.	Node of the grid, viewed at 1 kV, magnification 100X, after 2 h 30 min at 150°C.

Fig. 2-7 Effect of temperature on charge retention in quartz fabric.

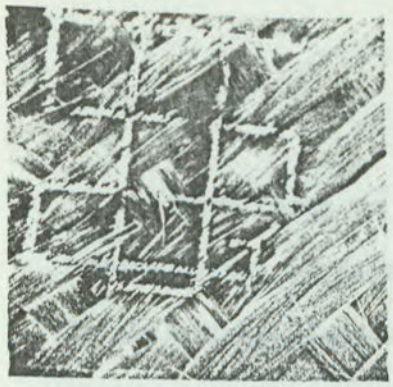
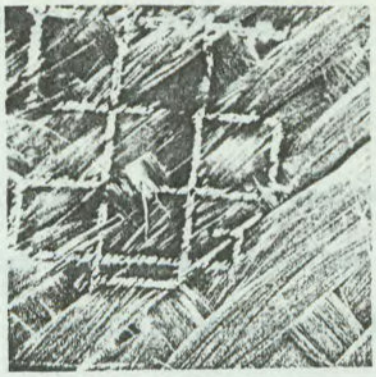
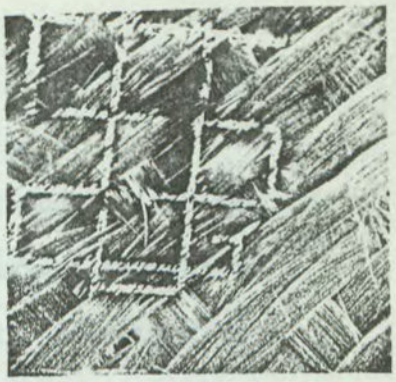
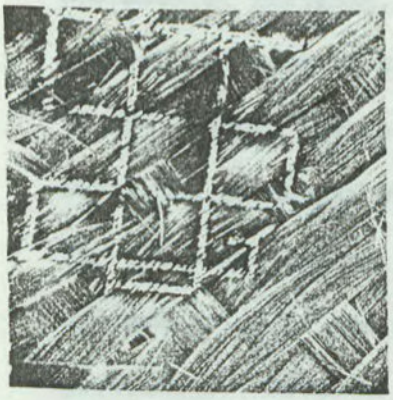
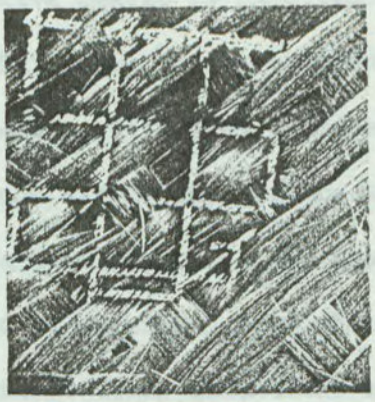

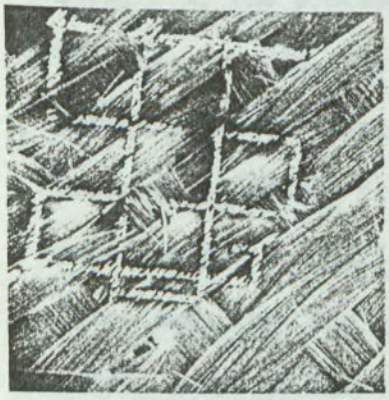
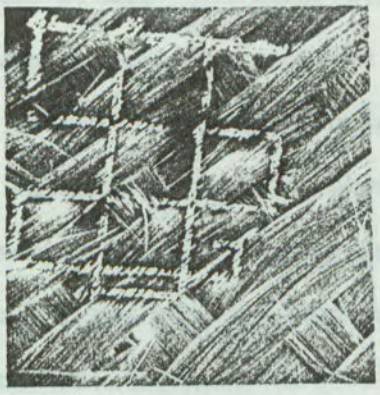



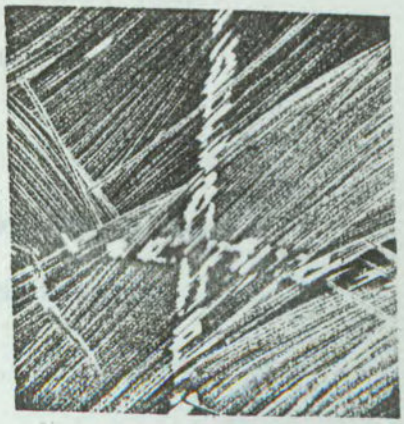

3. MICRO-DISCHARGES

M. Cuchanski

A stationary or slowly travelling focussed beam produces discharge events which, to distinguish them from discharges involving large areas, we call micro-discharges. A probable mechanism of their production is based on the one-dimensional theory of Meulenberg [1975]. In the first instants of charging, negative charge is injected into the dielectric to a depth of about 10 μm(20 keV beam) and is trapped there. As the amount of the trapped charge increases, it begins to repel and decelerate the impinging electrons which now strike the surface at a smaller velocity. The effective energy of the beam decreases and the surface may find itself on that point of the secondary emission curve which causes it to charge positively. After a few oscillations around the equilibrium point $N_s/N_i = 1$, the process should finally stabilize itself. Before this happens, however, a breakdown between the positive upper layer and the buried negative charge may occur. The breakdown is accompanied by a drainage of charge from an extended subsurface area surrounding the puncture point, and it causes an explosive ejection of electrons into space away from the surface. These emitted electrons were observed as sudden jumps of the electron collector current at the moment of a discharge. A strong discharge is usually followed by a few weaker ones of diminishing amplitude, and an interval of time (seconds to minutes) must elapse before another major discharge occurs.

The first measurements of the micro-discharges were made in the frequency domain [Balmain, Orszag, and Kremer, 1976], the spectra

obtained indicating nanosecond pulses. For measurements in the time domain we used a 4 GHz (rise time < 95ps) sampling oscilloscope in the setup shown in Fig. 3-1.

A sampling oscilloscope is designed to measure repetitive identical waveforms. It samples the incoming pulses at successive time intervals, the first pulse being sampled at $t = 0$, the second at $t = \Delta t$, the third at $t = 2\Delta t$, etc., in the pulse time frame, and displays the sampled amplitude as a dot on the oscilloscope screen. At a high sampling rate (Δt very small), the dots coalesce and we see what appears to be a continuous waveform. A sampling oscilloscope is not well suited for measurement of random amplitude pulses, but if the pulses have the same shape and differ in amplitude only, and if there exists an upper bound on the peak amplitude, the measurement difficulty can be circumvented by inserting attenuators in the trigger-signal path to raise the trigger treshold. The strongest pulses only are then sampled, and the pulse envelope can be obtained.

Pulses measured with this technique are shown in Fig. 3-2. Their peak amplitude is about 100 mA, the rise times vary from 0.2 to 0.5 ns (with similar fall times) and the pulse width is from 2 to 3 ns. The energy expended in the measurement line during a discharge is approximately 1.5×10^{-9} J.

The upper bound on the peak amplitude of micro-discharge pulse is related to the amount of charge mobilized in a discharge, and the rate at which the charge is released. The amount of charge, determined in

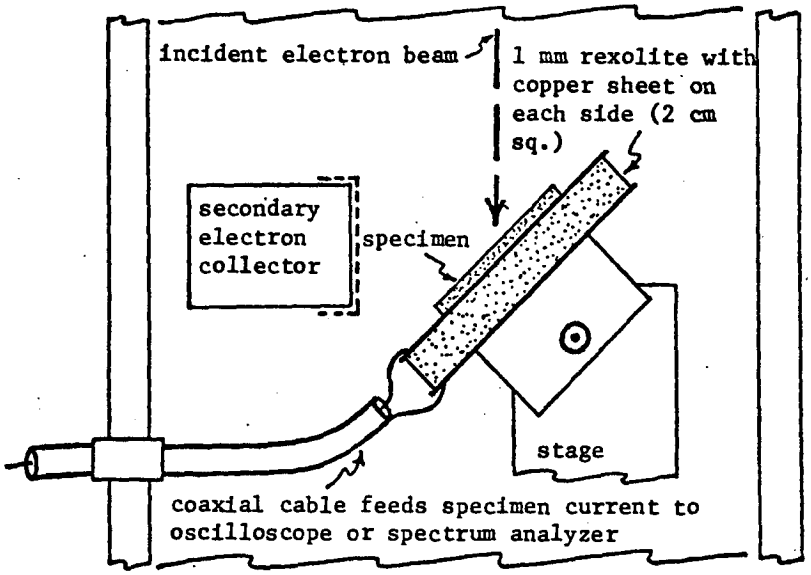

Arrangement of components in specimen vacuum chamber of scanning electron microscope.

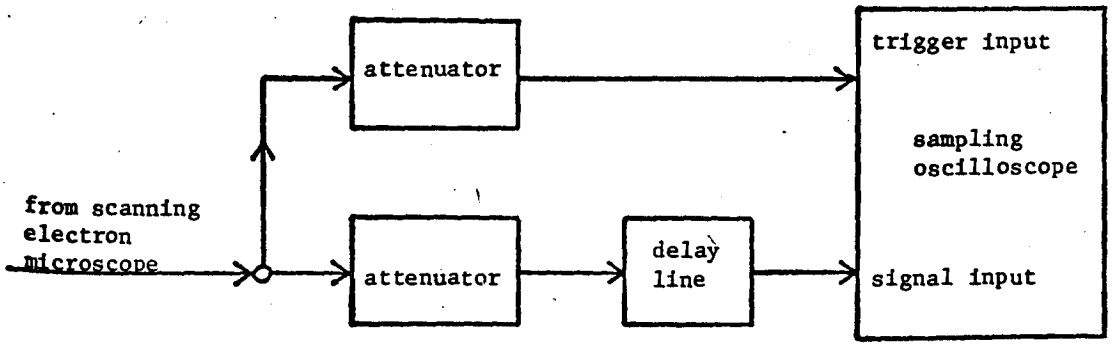

Fig. 3-1 Experimental setup for measurement of micro-discharge pulses

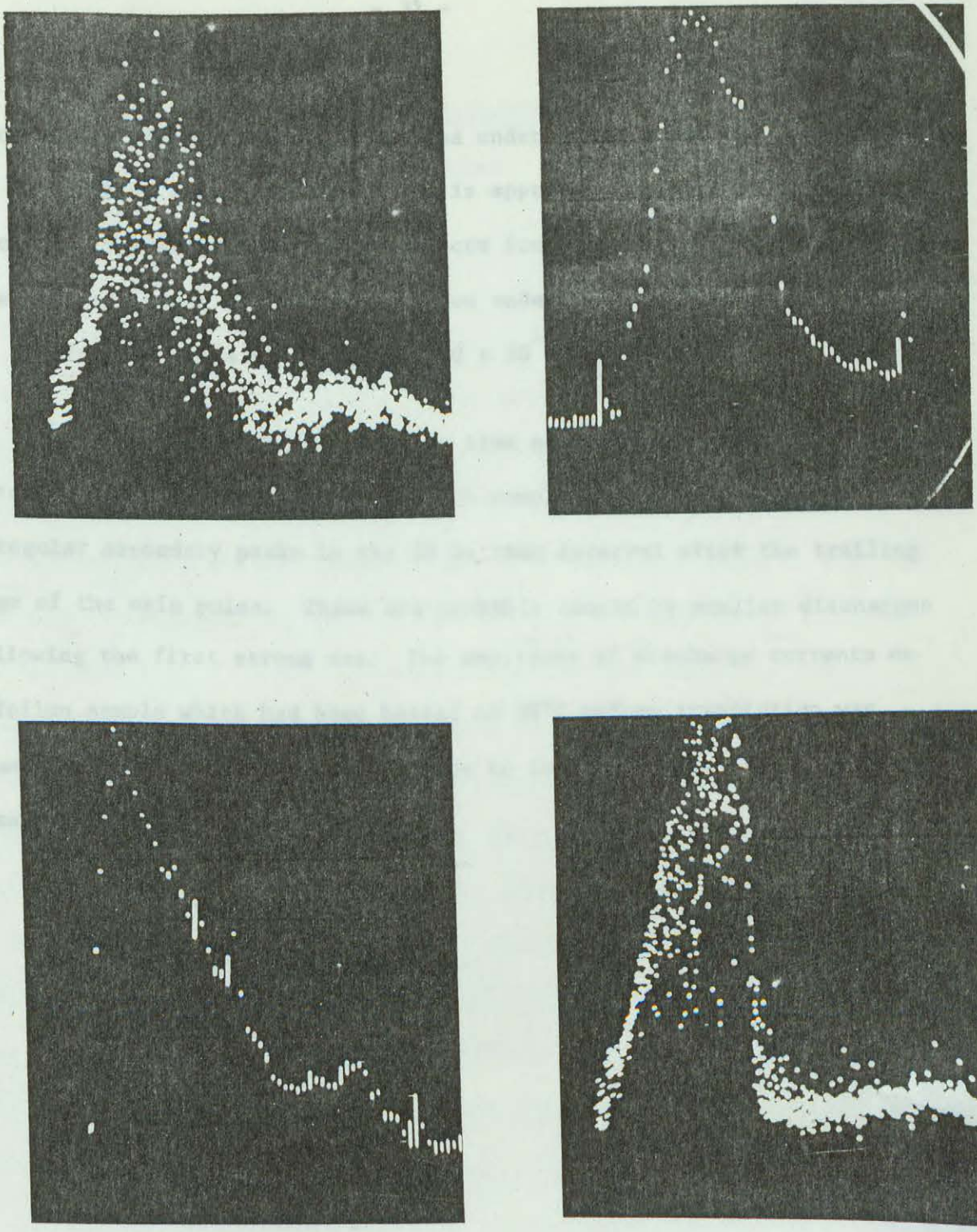

Fig. 3-2 Micro-discharge pulses on Teflon. The beam accelerating voltage is 18kV, the peak amplitude is 90 mA, and the time axis scale is 1 ns/div.

turn by the effective irradiated area under a spot beam, can be estimated by integrating a current pulse, and is approximately 3×10^{-10}C. Since the effective irradiated area had been found to be $5.0 \times 10^{-9} m^2$, then assuming a uniform charge distribution under the beam, the charge density an instant before a discharge is $6.0 \times 10^{-6} C/cm^2$.

The peak amplitude and the rise time seem to be independent of the material. Measurements made on Kapton samples showed a number of irregular secondary peaks in the 10 ns time interval after the trailing edge of the main pulse. These are probably caused by smaller discharges following the first strong one. The amplitude of discharge currents on a Teflon sample which had been heated to 38°C before irradiation was found to decrease by a factor of three to four but other pulse parameters remained the same.

4. MACRO-DISCHARGES

K. G. Balmain

4.1 Apparatus

A scanning electron microscope can be made to produce a broad, fairly uniform beam of electrons by removal of the final aperture, adjustment of the deflection coils and disconnection of the scanning coils. The SDT-SEM was set up in this way and its chamber modified to hold dielectric-sheet specimens up to 4.5 x 4.5 cm, as shown in Fig. 4.1. With this arrangement typical specimen current densities at 20 kV beam voltage were 1 to 2 $\mu A/cm^2$. Also shown in the same figure is the electrical diagram of the apparatus used for measurement of discharge current pulses. The coaxial components must have adequate energy ratings for pulsed signals; the energy rating is determined by multiplying the peak power rating by 5 μs (a time duration which appears to be an industry standard). A survey of manufacturers' specifications revealed that Weinschel attenuators have particularly high ratios of peak-to-average power ratings, and therefore are excellent for pulse measurements. The oscilloscope used was specified as having a 250 MHz passband.

4.2 Experimental Results

A typical discharge arc can be seen in Fig. 4.2(a) as a "lightning stroke" extending from the central region to the lower edge of the specimen. The other rays extending outward to the edges are not arcs

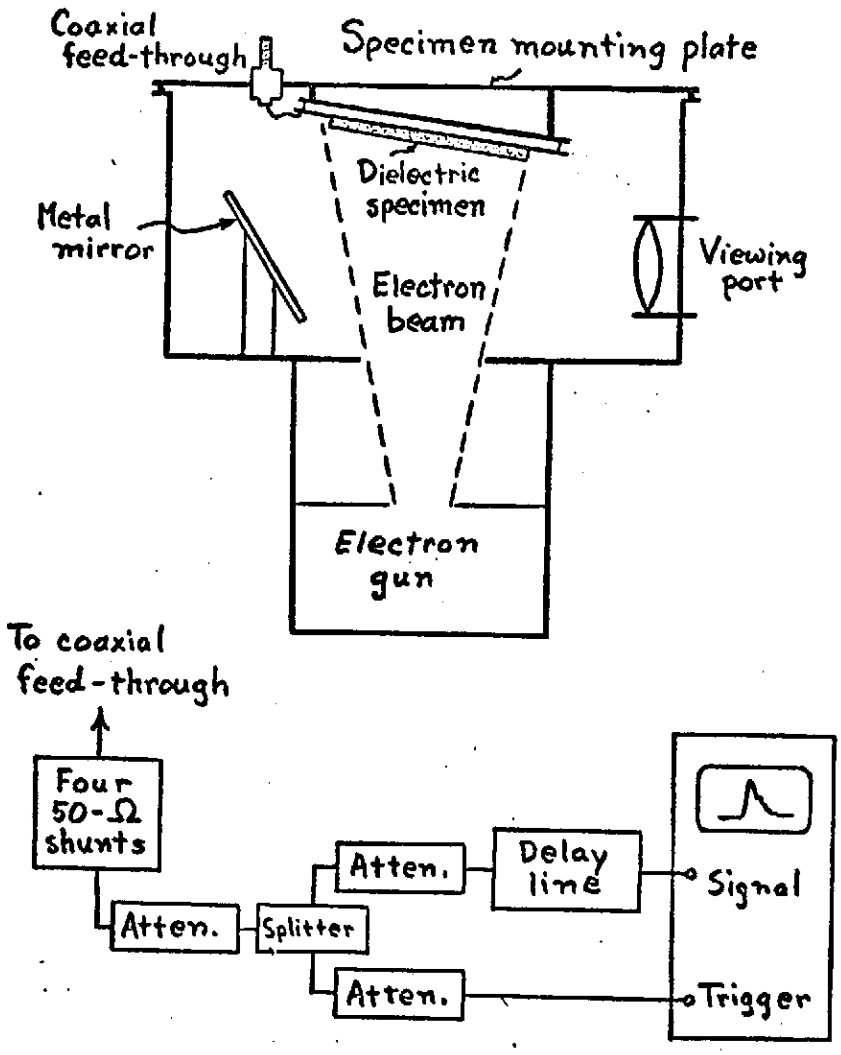

Fig. 4-1 The current-pulse measurement system using the flood-beam mode in the SDT SEM.

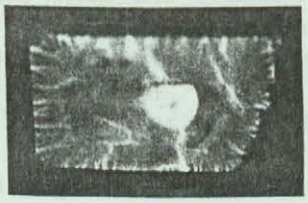

(a) Mylar specimen 48x26x0.12 mm, showing central illuminated region and arc going to lower edge.

(b) Same specimen as at left, showing arc traversing illuminated region and going to upper edge.

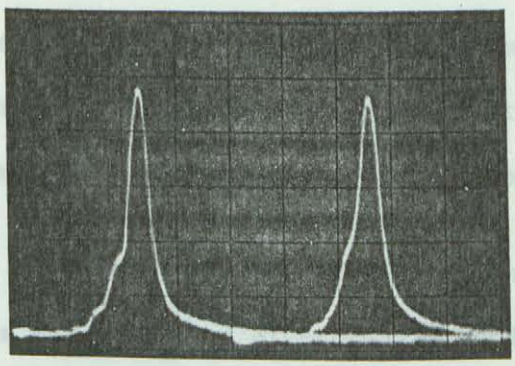

(c) 100 A peak current pulses on a 10 cm^2 Mylar specimen 0.1 mm thick. Hor. scale 50 ns/div.

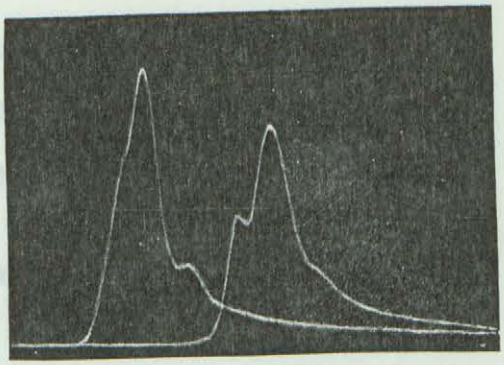

(d) Quartz fabric discharges of 1.6 A and 1.3 A peak on a specimen of 2 cm^2. Hor. scale 50 ns/div.

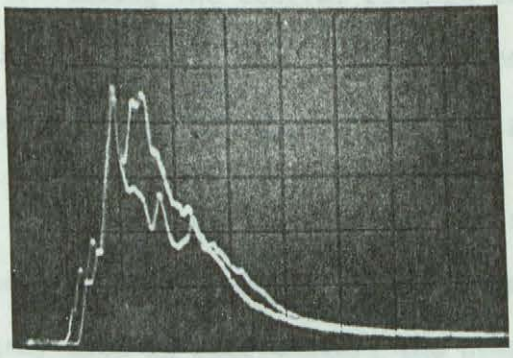

(e) Silvered-Teflon discharges of 20A peak on a specimen of 10 cm^2. Hor. scale 50 ns/div.

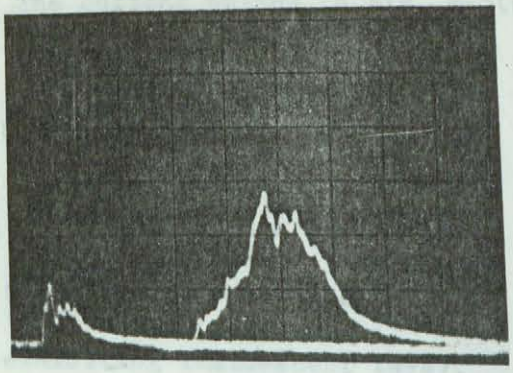

(f) Aluminized-Kapton discharges on a 5 cm^2 specimen, at 100 ns/div. Large pulse: 9A peak.

Fig. 4-2. Examples of macro-discharges on various materials, with an incident-beam accelerating voltage of 20 kV.

but rather luminescence which appears for a short period after each discharge, when the reduced negative surface charge permits the incident electrons to reach the dielectric surface with appreciable energy. The central bright spot is illumination from the filament of the electron gun. In Fig. 4-2(b) an arc can be seen crossing the bright spot, thus indicating that the filament illumination is not strong enough to discharge the specimen by photoemission.

The strongest discharge currents measured to date, 100 A peak, are shown in Fig. 4-2(c). Also shown in Fig. 4-2(d), (e) and (f) are typical discharges on quartz fabric, silvered-Teflon second-surface mirror, and aluminized-Kapton thermal blanket outer layer.

One silvered-Teflon specimen had its central region covered with a carbon-filled electrically conductive sponge material, in order to reduce light reflection from the filament into the viewing port. This produced the unexpected result of increased complexity in the discharge arc. For example, in Fig. 4-3(a), arcs appear in a complex web pattern surrounding the central covered region. The current pulses in Fig. 4-3(b) through (f) are also relatively complex, often seeming to consist of multiple pulses, each perhaps triggered by the one before.

It may be relevant to the foregoing observations that the incident beam scarcely touched the specimen edge (the beam covers the circular gray area in Fig. 4-3(a), the beam edge exhibiting luminescent rays). Perhaps the arc could not traverse the electron-deficient area near the specimen edge.

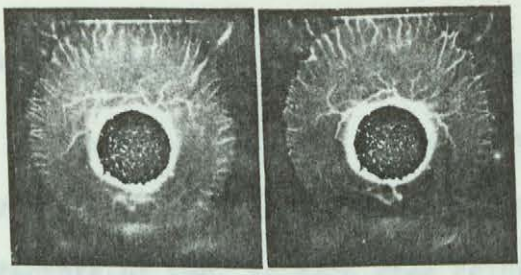

(a) Discharge arcs in the region exposed to the electron beam. The specimen is 4.5 x 4.5 cm.

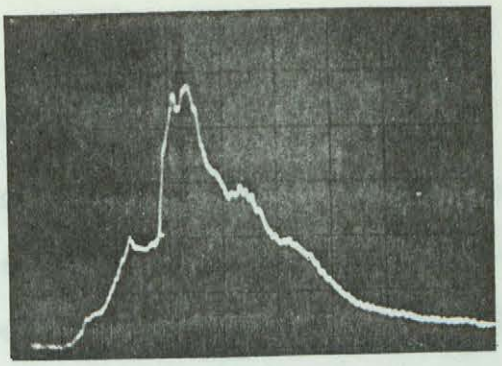

(b) Current pulse, 10.5A peak, 100 ns/div.

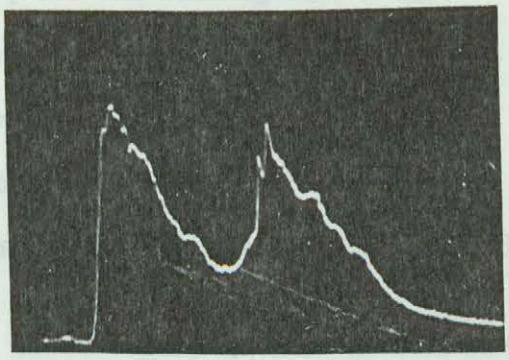

(c) Current pulse, 10A peak, 100 ns/div.

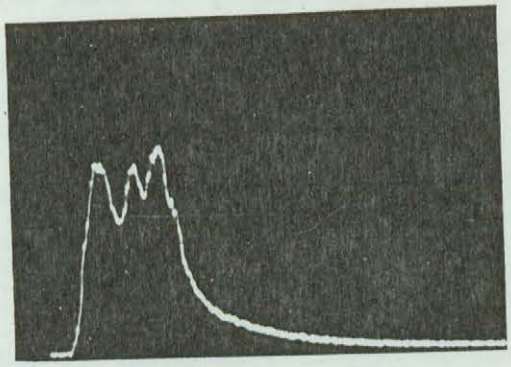

(d) Current pulse, 9A peak, 100 ns/div.

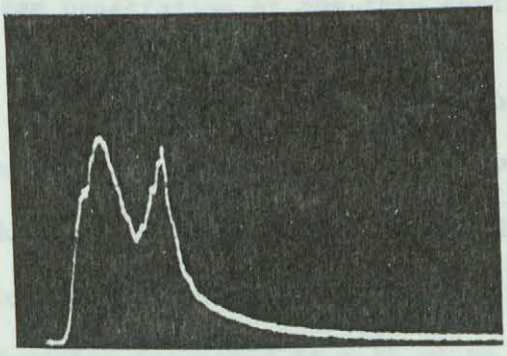

(e) Current pulse, 9A peak, 200 ns/div.

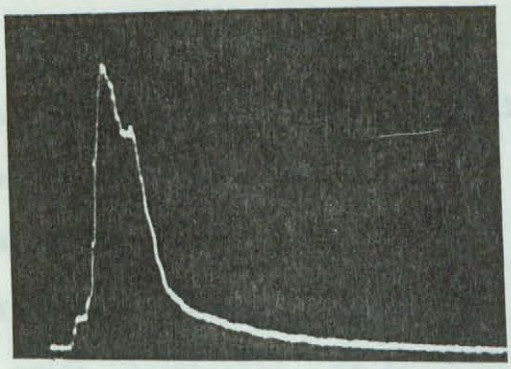

(f) Current pulse, 11A peak, 200 ns/div.

Fig. 4-3. Discharges on silvered-Teflon with central region covered by a conducting disc. The incident beam accelerating voltage is 20 kV.

4.3 Discharge Scaling With Specimen Area

In order to study the phenomenon of "charge cleanoff", experiments were conducted in which a specimen was sequentially cut down in area by factors of two, at each step being exposed to the flood beam of electrons. For each such step at least six discharge current pulses were recorded and their peak currents averaged. The silvered-Teflon results of Fig. 4-4(a) for the first run (in which the specimens were alternately square and rectangular) suggest a definite power-law relationship between peak current and area. A second run (square specimens only) was not significantly different. A specimen of 0.85 mm thick white Teflon PTFE did not exhibit this scaling effect, having discharges with peak currents around 1 A independent of area.

Similar experiments on copper-clad Mylar revealed the possibility of thickness dependence. Fig. 4-4(b) shows that the thicker specimen exhibits by far the greater discharge current. The reasons for this are not clear although conceivably they could involve occasional electron beam penetration of the thin specimen.

It was also observed that the discharge pulse duration is not simply related to the area. In the silvered-Teflon experiments the pulse duration (at half peak current) increased very erratically from 15 ns to 100 ns with increasing area. However for the 0.1 mm Mylar, the duration increased from 15 ns to 25 ns, again erratically. It is difficult to draw conclusions from these pulse duration observations although it can be said that the dielectric arcs bear little resemblance to capacitor discharges.

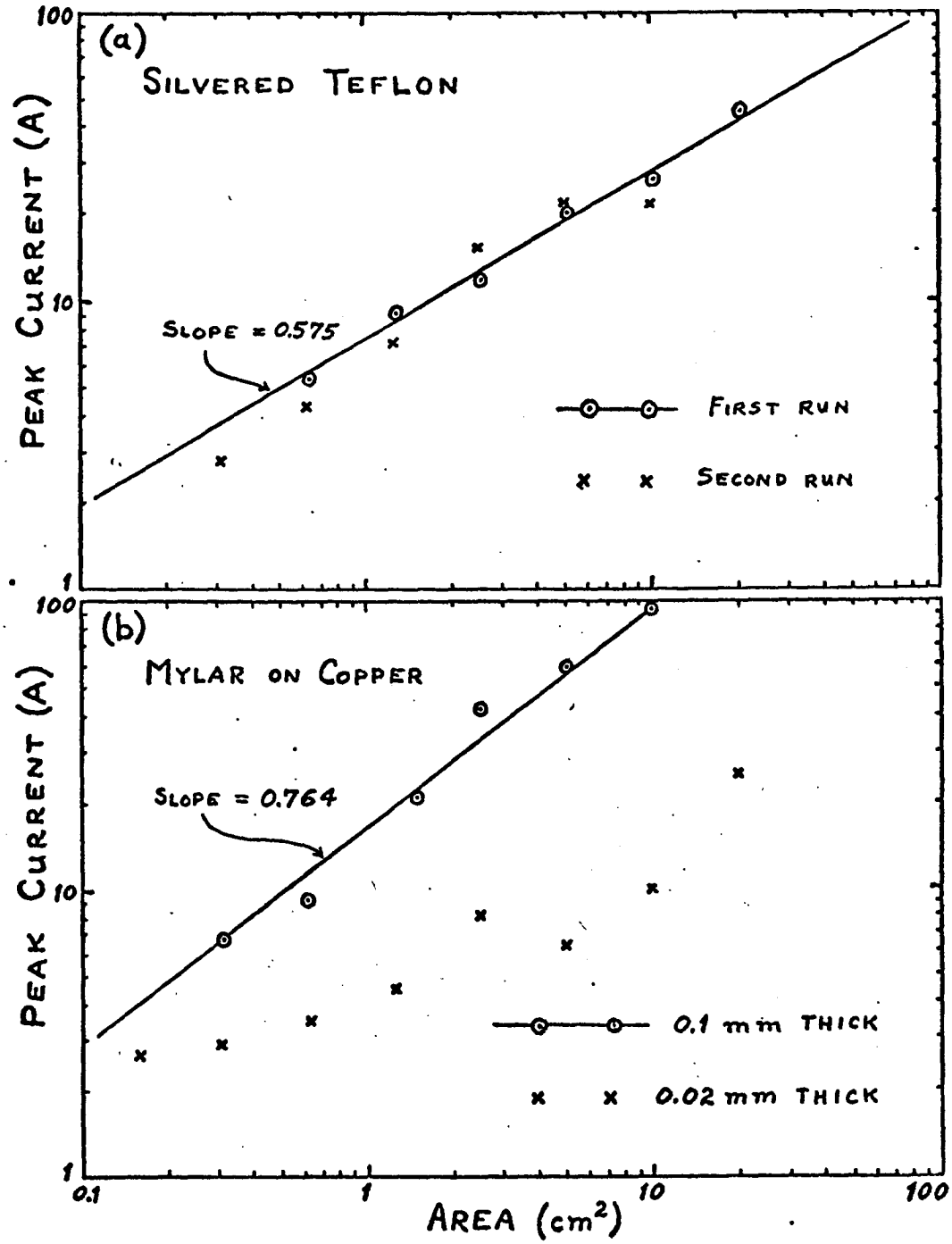

Fig. 4-4 The scaling of discharge peak current with specimen area, for a 20 kV beam.

The power-law relationship of peak discharge current to area can be extrapolated as shown in Fig. 4-5. The effective areas of micro-discharges were estimated from charge imaging techniques applied to focussed and slightly defocussed beam "tracks" on exposed specimens. It is interesting to note that the power-law curve passes through the micro-discharge region, indicating that micro- and macro-discharges could be merely different magnitudes of the same basic phenomenon.

4.4 Specimen Shape Factor

The possible existence of a shape factor (or geometrical factor) has to be considered in relation to peak-current scaling. Covering a circular region with a conducting material as depicted in Fig. 4-3 had the effect of producing complex, multiple and reduced-amplitude discharge pulses. With regard to Kapton thermal blanket material, a perforated specimen was found to produce lower amplitude discharges than a non-perforated specimen but the number of experiments performed was not adequate for a proper comparison. In many experiments the arcs were observed visually to extend to the edge of the specimen, suggesting that the edge may play some sort of very specific role in the discharge process.

In an attempt to be more quantitative, a rectangular specimen of 0.1 mm thick Mylar measuring 1.25 x 4.00 cm was studied. The average peak current over six discharges was 22 A which is appreciably less than the currents measured for other specimens of the same 5 cm^2 area, shown in Fig. 4-4(b). In fact, the 22 A measured would seem to be

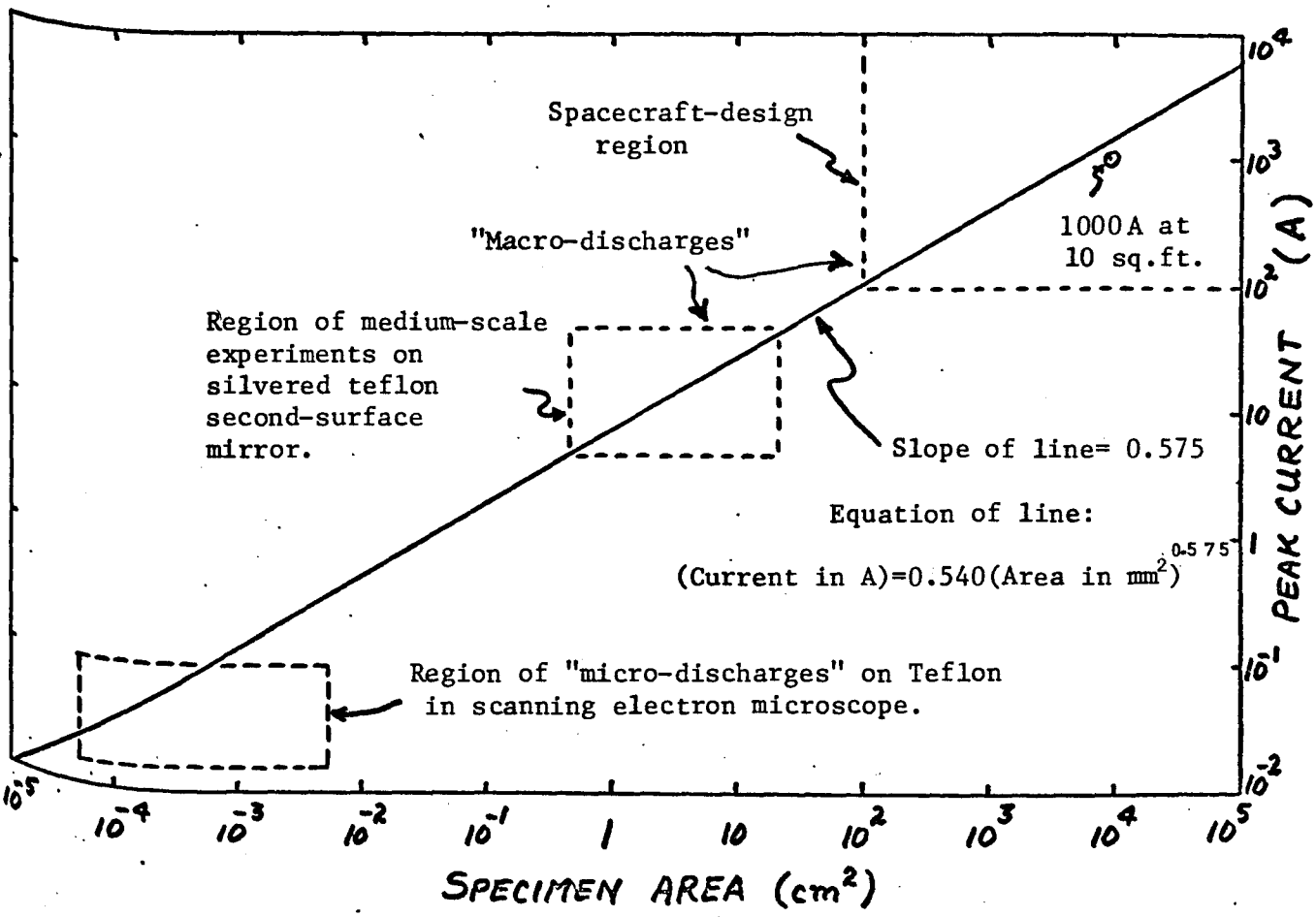

Fig. 4-5 Peak discharge current as a function of dielectric area, for a 20 kV beam.

more appropriate for specimens of 1.5 to 1.6 cm^2. Visual observations indicated arcs going preferentially to the long edges of the specimen.

Another instance of possible shape effect can be seen in Fig. 4-4(a) in which the"first run" involved alternate square specimens and rectangular specimens with a 2:1 side ratio. The points lying below the straight-line average were all rectangular. However, the fluctuations in this type of experiment are such that this result cannot be regarded with certainty as being due to specimen shape.

4.5 Physical Damage

Prolonged exposure of any specimen to the electron beam produces a faint brownish surface coloration. Sometimes, particularly for small specimens, the discharge amplitude and frequency of occurrence decrease with time. Particularly on Mylar specimens surface damage and punch-through have been noted, but always such damage appears to be associated with existing surface scratches. Punch-through on copper-clad Mylar specimens sometimes produced a tiny "blob" of melted copper, which could be seen with the aid of a 10-power magnifier.

5. ELECTROMAGNETIC WAVE ATTENUATION IN A CHARGED DIELECTRIC

K. G. Balmain

5.1 Introduction

The possibility of electromagnetic wave attenuation and phase shift by charge accumulation in a dielectric sheet stretched across a dish or horn antenna was suggested by Dr. J. V. Gore. With such an arrangement, the dielectric would be some distance from the metal antenna and without metallic backing adjacent to the dielectric sheet, accumulated charge in the sheet would not have a nearby "image" charge. Therefore the accumulated negative charge would tend to repel strongly any electrons in the vicinity and high charge densities would not build up. This was established experimentally in the SDT SEM by mounting test specimens of dielectric on a Plexiglas specimen plate rather than on a metal plate; no discharges were observed using the Plexiglas plate. Because RF effects due to the accumulated charge were expected to be small, it was decided to maximize charge accumulation by using experimental geometries with grounded metal either adjacent to or close behind the dielectric, that is to use geometries with nearby image charges.

5.2 The Lumped-Charge Experiment

This experiment involved electron irradiation of the Teflon dielectric at the open-circuit end of a coaxial resonator, while measuring the Q of the resonator. The basic experiment was set up as in Fig. 5-1(a) using

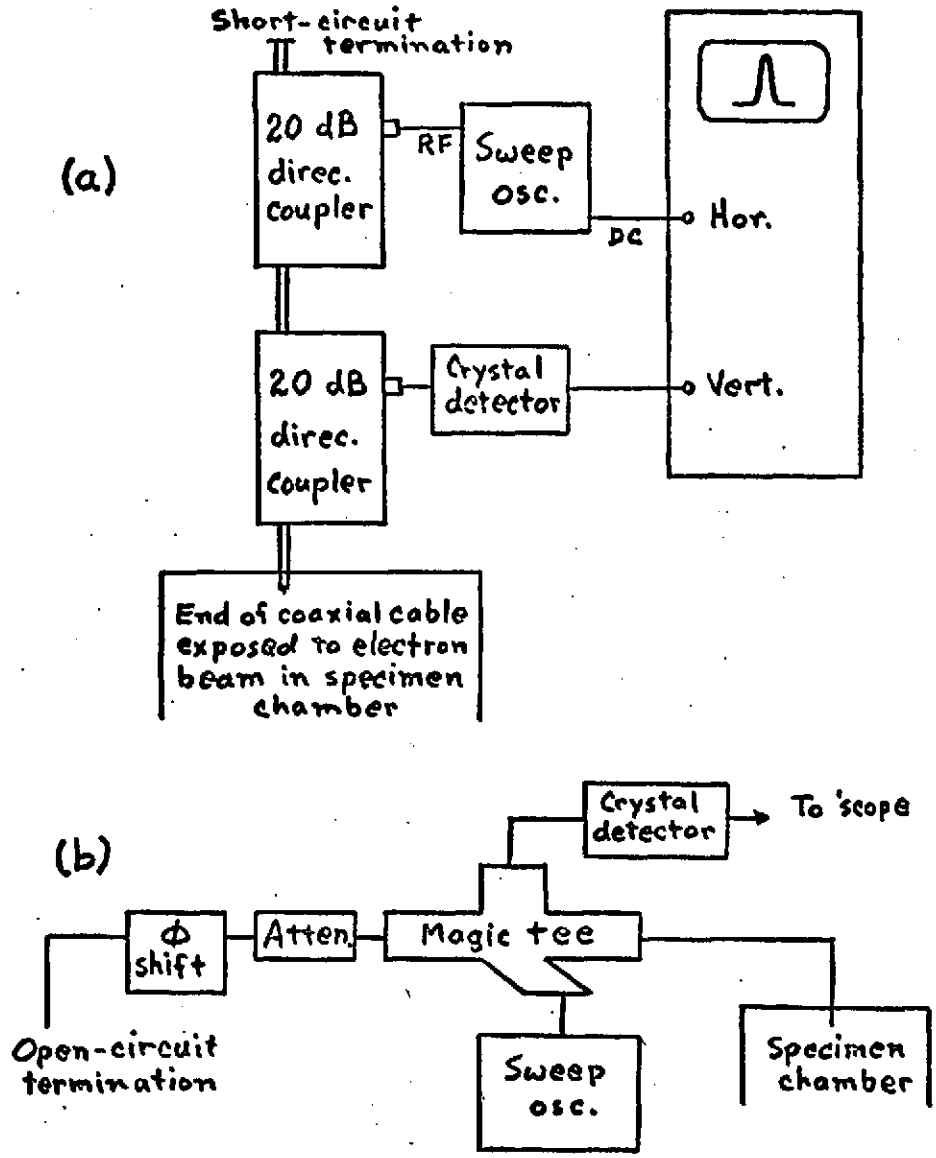

Fig. 5-1 Apparatus for the lumped-charge experiment on measurement of RF absorption in a charged dielectric for (a) 0.5-1.0 GHz and (b) 7-12 GHz.

directional couplers designed for the range 0.5 to 1.0 GHz. The transmitted signal goes through a sharp peak at resonance, the sharpness of the peak being closely related to the resonator Q factor. Under electron bombardment, no change in the peak was observed, that is no change in its frequency, width or height. Tiny arc discharges were clearly visible on the Teflon, so the dielectric was certainly being charged as much as possible. The "magic-tee" termination comparator circuit of Fig. 5-1(b) was set up using X-band waveguide, and similarly no effect was observed for the frequency range 7-12 GHz.

An analysis of this null result was carried out by Maasland [1977] who determined the smallest resistive load addition to the coaxial resonator which would just escape detection, given the noise level of the system. This gave a conductivity-thickness product σ t for a postulated conductive region created by electron bombardment of the end of the coaxial cable. The uniform plane wave attenuation by a conductive layer with the same σ t product was then calculated and found to be less than 10^{-3} dB in the frequency range 0.5 - 1.0 GHz.

5.3 The Distributed-Charge Experiment

In an attempt to accentuate any effect due to accumulated charge, a copper-on-Mylar stripline section attached to the end of the resonator was exposed to the electron beam, as shown in Fig. 5-2. This meant that the fringing field of the stripline could interact with the embedded charge over a distance of 42 mm. With this arrangement the resonator Q was observed to decrease during electron bombardment. This effect

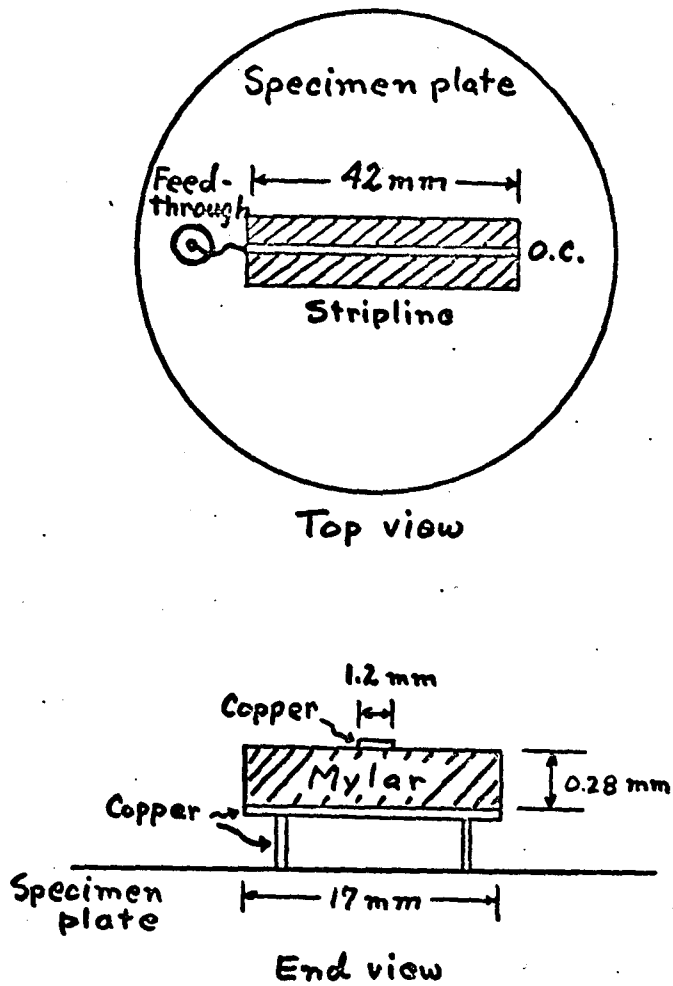

Fig. 5-2 The modification used for the distributed-charge stripline experiment.

took a few seconds to build up after the electron beam was turned on and a few tens of seconds to return to normal after the electron beam was shut off. More specifically, the magnitude of the resonant-peak power transmitted through the resonator system was lowered between 4% and 7% for the three resonances occurring in the range 0.5-1.0 GHz. No shift in resonant frequency was observed. Qualitatively similar results were observed in the frequency range 7-12 GHz, using the magic-tee comparator.

The above power loss measurements could not be translated into attenuation values for a uniform plane wave normally incident on a thin conducting sheet, because an appropriate theoretical analysis of the lossy stripline was not available. Nevertheless it is clear that the uniform-plane-wave attenuation would be very small indeed.

6. PULSE PROPAGATION

M. Cuchanski

As the first step in the simulation of electromagnetic pulse propagation on spacecraft structures, we looked into transmission between two monopoles mounted on a solid ground plane. Attention was focussed on the signal fidelity, edge reflection effects, and the use of lossy materials. Experience gained in these exploratory measurements (carried out by Mr. J. Nkeng) was of a great assistance when, in order to have a structure closer resembling a solar-array "sail", we replaced the ground plane with a wire grid. In the experiments with the wire grid, we were able to isolate and identify antenna and grid resonances excited by a pulse.

Edge effects for pulse transmission between two monopoles over a ground plane are shown in Fig. 6-1 (the monopoles were 15 cm long and 72.5 cm apart, the ground plane was made of a 151.6 x 91.5 cm aluminium sheet). The top trace is the received signal when no lossy material was present, the bottom one was obtained when strips of Eccosorb LS22 were laid down along the circumference of the plane. It is seen that the damping of edge reflections and edge currents on the plane results in a significant change of the signal: its amplitude and frequency increase, and it is phase-shifted relative to the first signal.

To eliminate pulse-excited antenna oscillations and in this way improve signal fidelity, a square "hat" made of the same lossy material was placed on the top end of each monopole. Fig. 6-2 compares the trace for transmission over ground plane between "loss-free" antennas with the

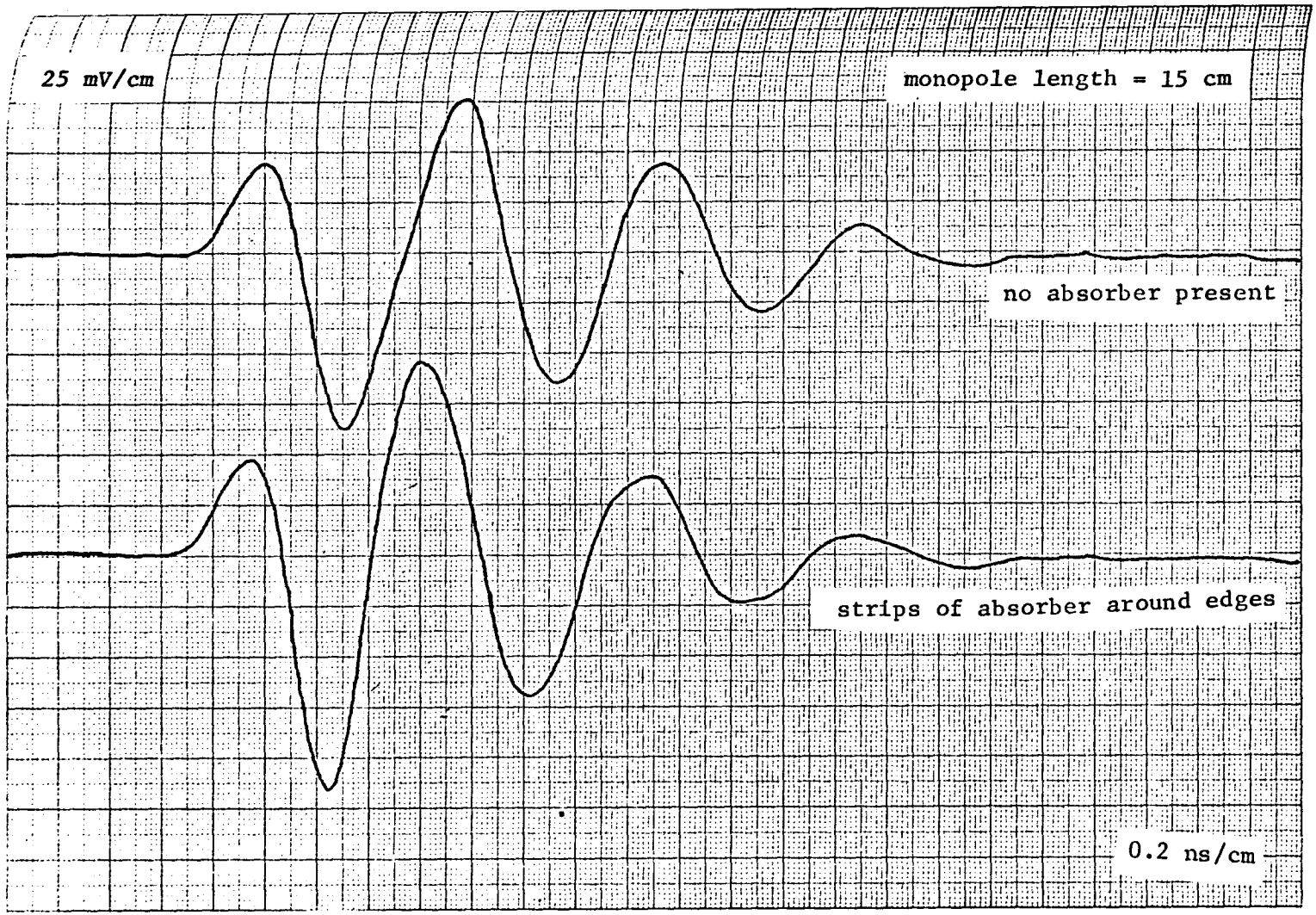

Fig. 6-1 Edge effects in transmission over ground plane.

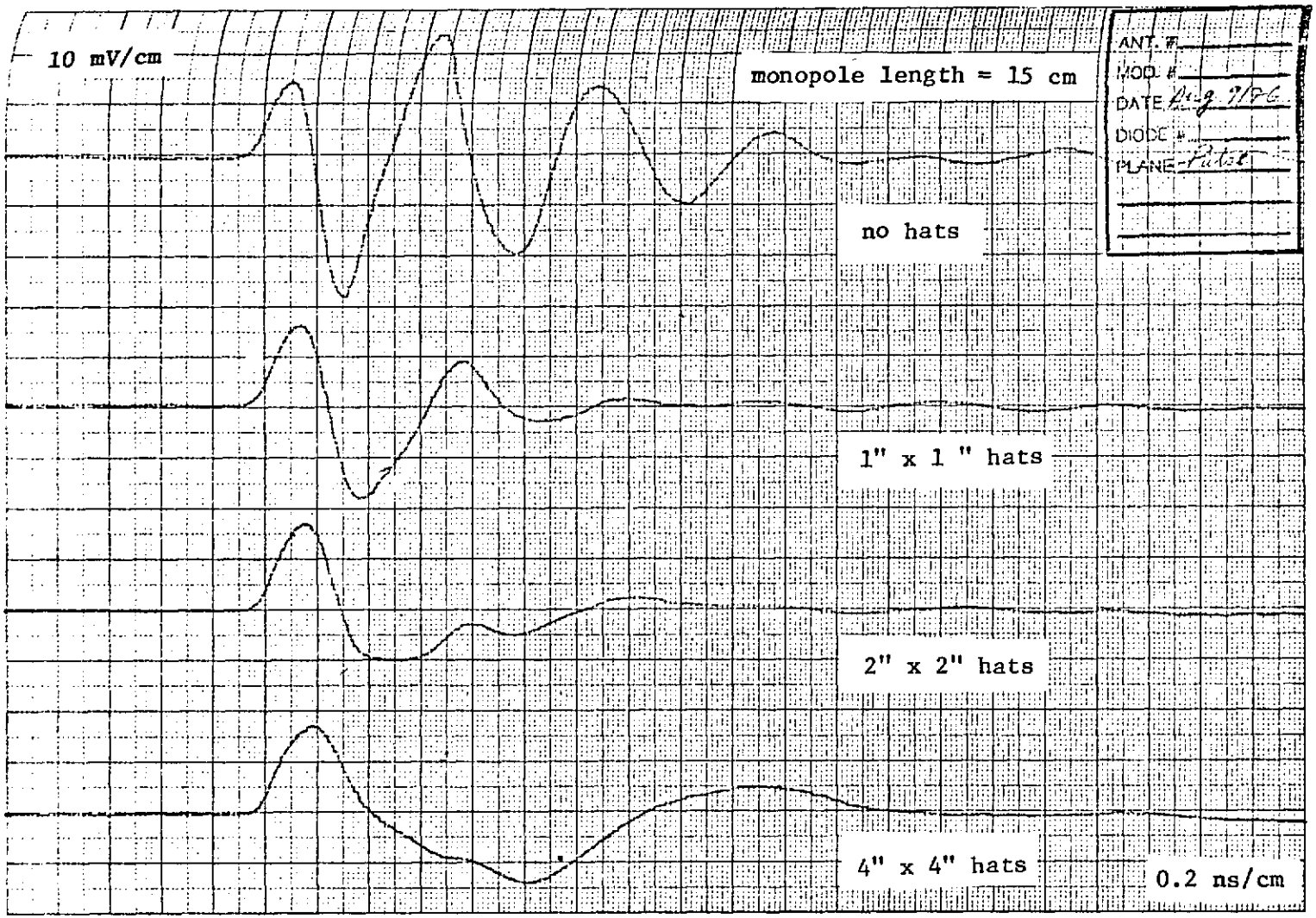

Fig. 6-2 Transmitted signal as function of hat size.

waveforms obtained when hats were used. As the size of the hats increases, the oscillations decrease in amplitude and decay faster. However, the derivative of the transmitted pulse is preserved fairly well. This result indicates that the combination of monopole plus lossy hat could be used for transmission of high speed pulses, or, for the spacecraft charging problem, such an antenna could be used to pick up with reasonable fidelity the radiation from an arc discharge.

The experimental setup for measurement of pulse transmission over a wire grid is shown in Fig. 6-3. The grid was made of square copper wire 3 x 3 mm in cross-section and bonded at the junctions. The monopole antenna were made of copper wire 0.95 mm in diameter and were mounted over an 11.6 x 11.6 cm brass plates soldered to the grid. The transmitting antenna was driven by an Ikor R100 impulse generator which produced 1 kV, 0.5 ns wide pulses at the repetition rate of 226 Hz; the low repetition rate guaranteed that the time between pulses was much longer than the time required for the entire system to return to a quiescent state. The output of the receiving antennas was monitored by a 4 GHz (rise time $\leq$ 95ps) sampling oscilloscope. The two antennas were identical in a given set of measurements, and four sets, corresponding to the monopole lengths of 5, 10, 15, and 20 cm, were obtained. The effects of introducting a lossy material (Eccosorb LS 22) at various points on the structure were observed for each antenna length.

A pulse sent by the transmitter can reach the receiver either along the direct path of length d (Fig. 6-4), or it can be reflected from an edge of the grid and arrive at a later time along one of the edge paths d_1 or d_2. The travel times are $\tau = d/c$, $\tau_1 = d_1/c$ and $\tau_2 = d_2/c$, where c is

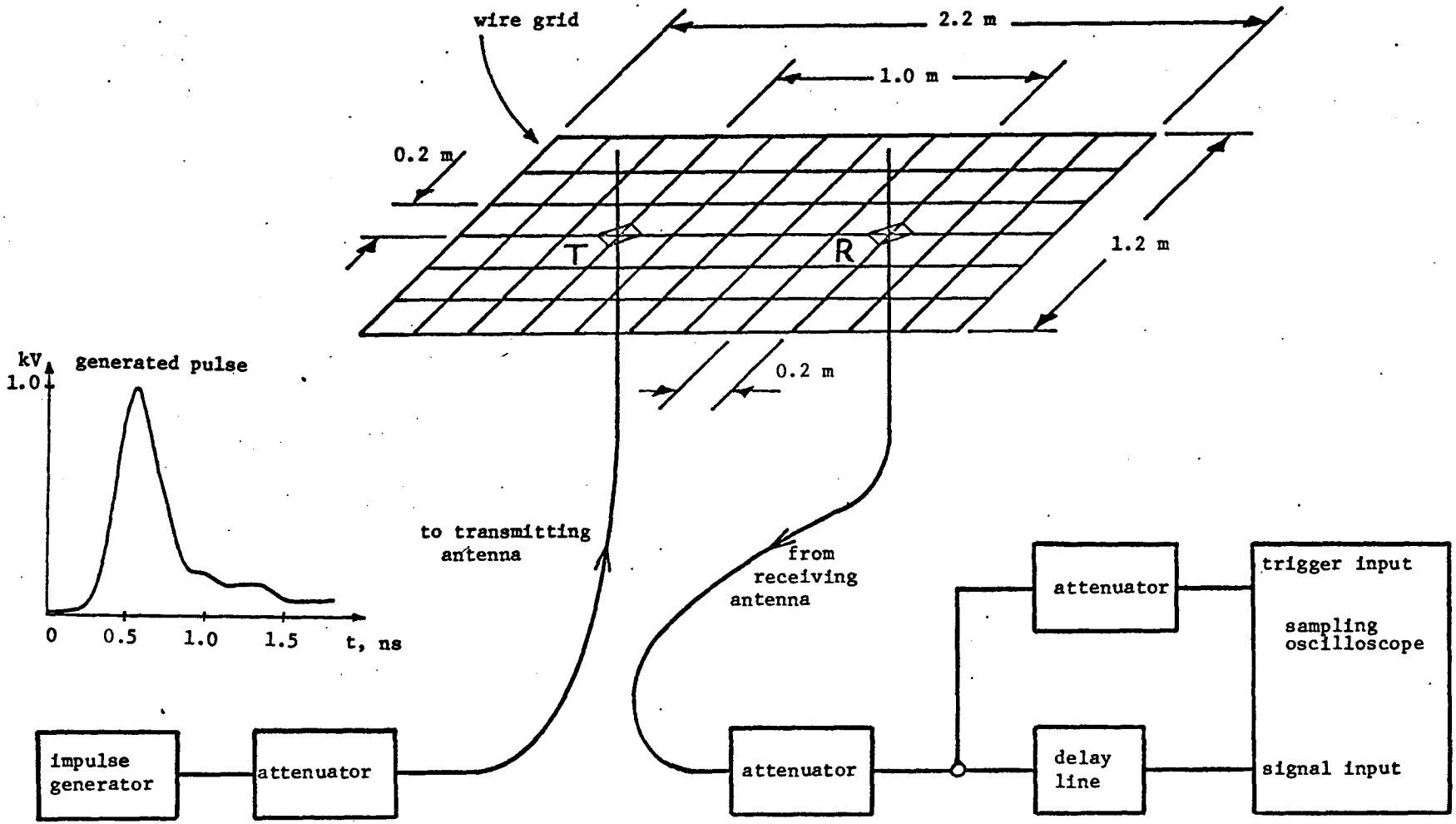

Fig. 6-3 Experimental setup for measurement of pulse transmission over wire grid.

the speed of light, and the delay times are $\tau_1 - \tau$ between a pulse and its reflection from the long edge and $\tau_2 - \tau$ between a pulse and its reflection from the short edge. The reflection from the short edge

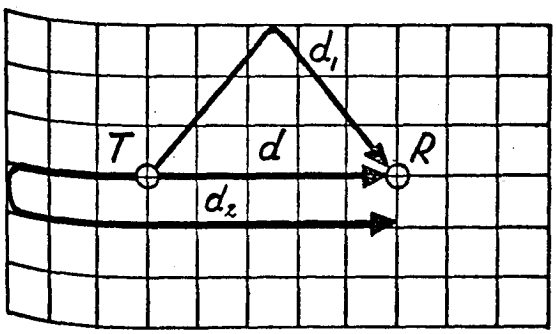

$d = 1.0$ m $\quad \tau = 3.33$ ns

$d_1 = 1.56$ m $\quad \tau_1 = 5.21$ ns $\quad \tau_1 - \tau = 1.87$ ns

$d_2 = 2.2$ m $\quad \tau_2 = 7.33$ ns $\quad \tau_2 - \tau = 4.0$ ns

Fig. 6-4 Signal paths, travel times, and delay times.

undergoes a high attenuation because of the longer transmission path, and is difficult to identify. The reflection from the long edge, however, has large enough amplitude and can be seen as a pulse arriving at a time $\tau_1 - \tau$ after the direct path pulse. If the antennas were able to transmit a pulse faithfully without going into oscillations, and if in addition the grid did not contribute its own oscillations, we would see the pulse and its two reflections as "clean" waveforms separated from each other by the delay times. Unfortunately, this is not so, and the signal at the receiver is the superposition of several signals of different origin.

A monopole excited by a pulse goes into oscillations because a pulse arriving from the generator is reflected from the top end of the antenna and then bounces back and forth between the end and the base.

The frequency of the oscillations is the natural resonant frequency of the antenna, i.e. it is related to the monopole length ℓ_a through $f_a = c/4\ell_a$. Fig. 6-5 compares the received signals for four monopole lengths. Each of the waveforms can be divided into three regions: 1. the build-up of a pulse on the antenna, 2. the release of the stored energy in a few high-amplitude, fast-decaying oscillations, 3. a long oscillatory tail of varying amplitude. The measured periods of oscillations in the region 2 are in a good agreement with the theoretical values of the natural resonant periods of the antennas; the oscillations can therefore be identified as antenna-originated.

A reflection from the long edge is best seen in the signal received by the 15 cm monopole. There the period of oscillations and the arrival time of the reflection had just the right values to cause a superposition of a large positive reflection on a negative half-cycle of the main sinusoid; the cancelled half-cycle had been $\tau_1 - \tau$ distant from the first pulse. For other monopole lengths the relative timings were less propitious; nevertheless the various kinks appearing on the otherwise smooth waveforms, for instance the one on the signal from the 20 cm monopole, can be traced down to reflections.

We developed another technique of studying the edge effects, one that offers an interesting alternative. Strips of a lossy material (Eccosorb LS 22) were laid on the edges to reduce the amplitude of reflections bouncing off them. The results of the measurements are shown in Fig. 6-6. As had been anticipated, the presence of the lossy material on the short edges had little influence on the received signal. When, however,

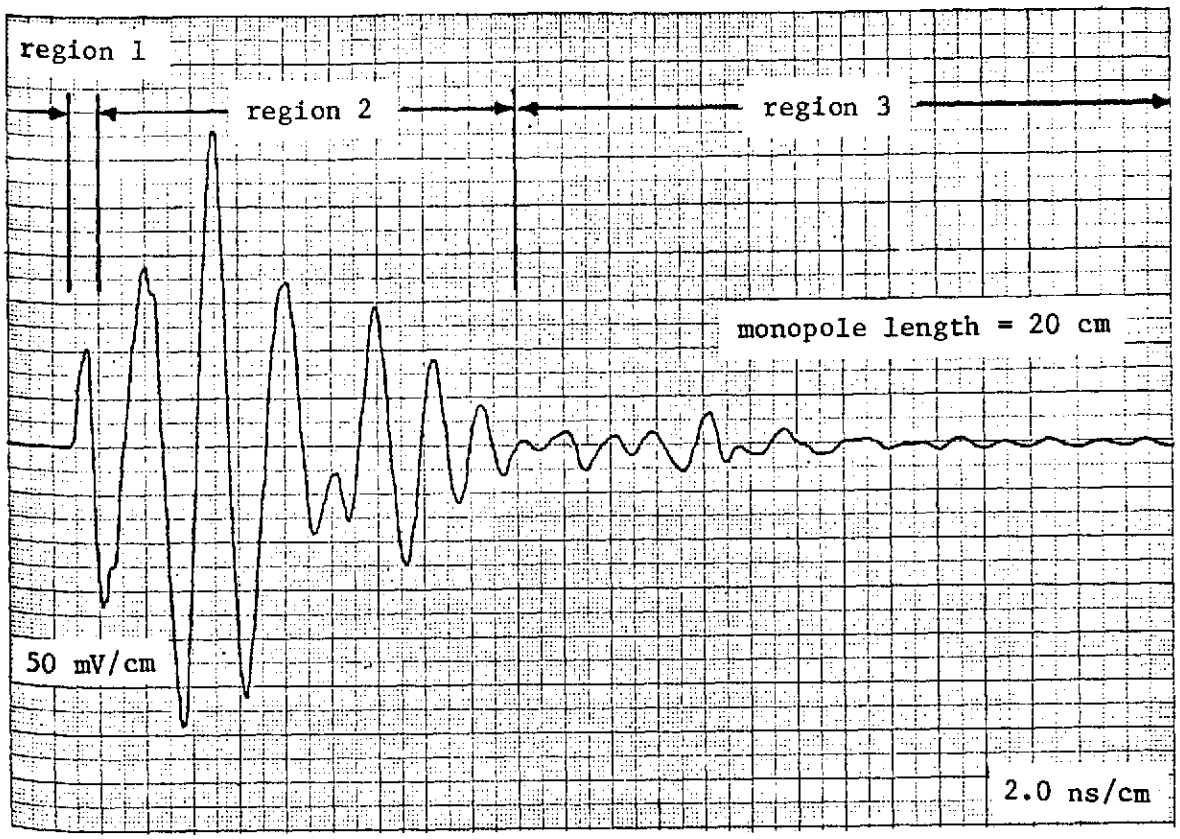

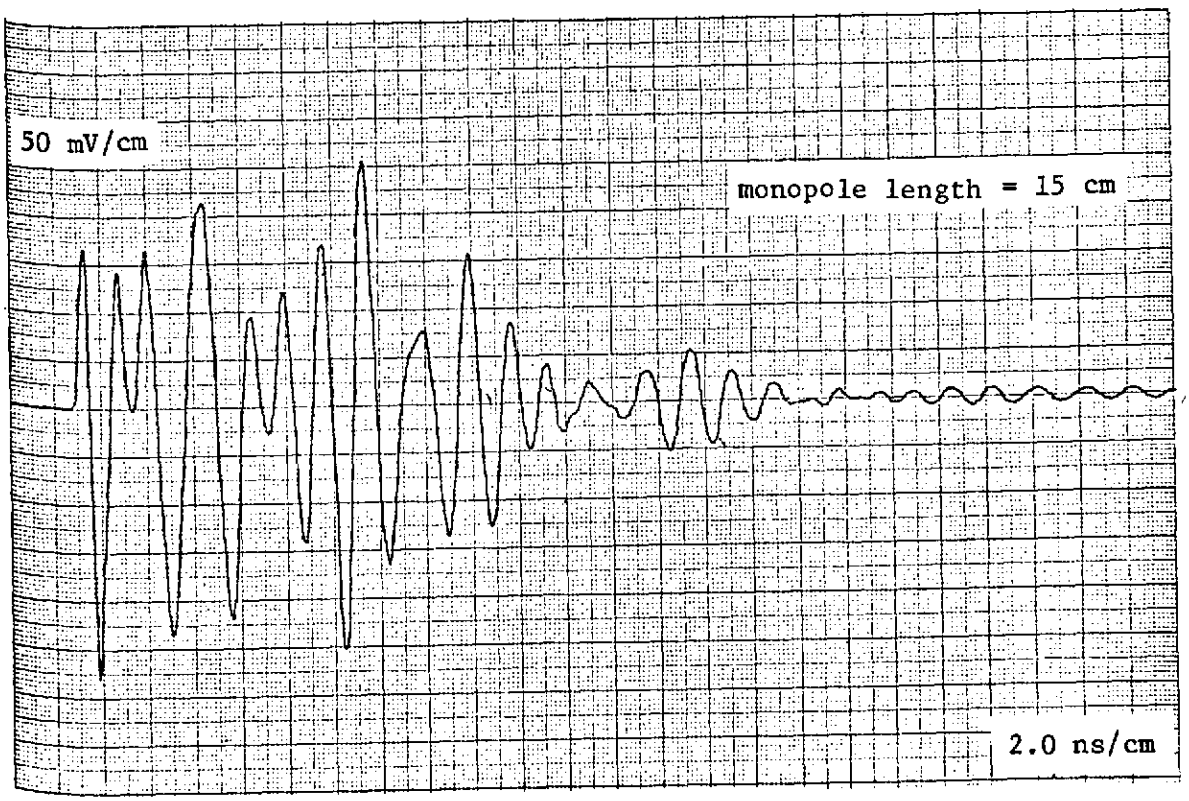

Fig. 6-5 a Comparison of received signals for four antenna lengths. No lossy material present.

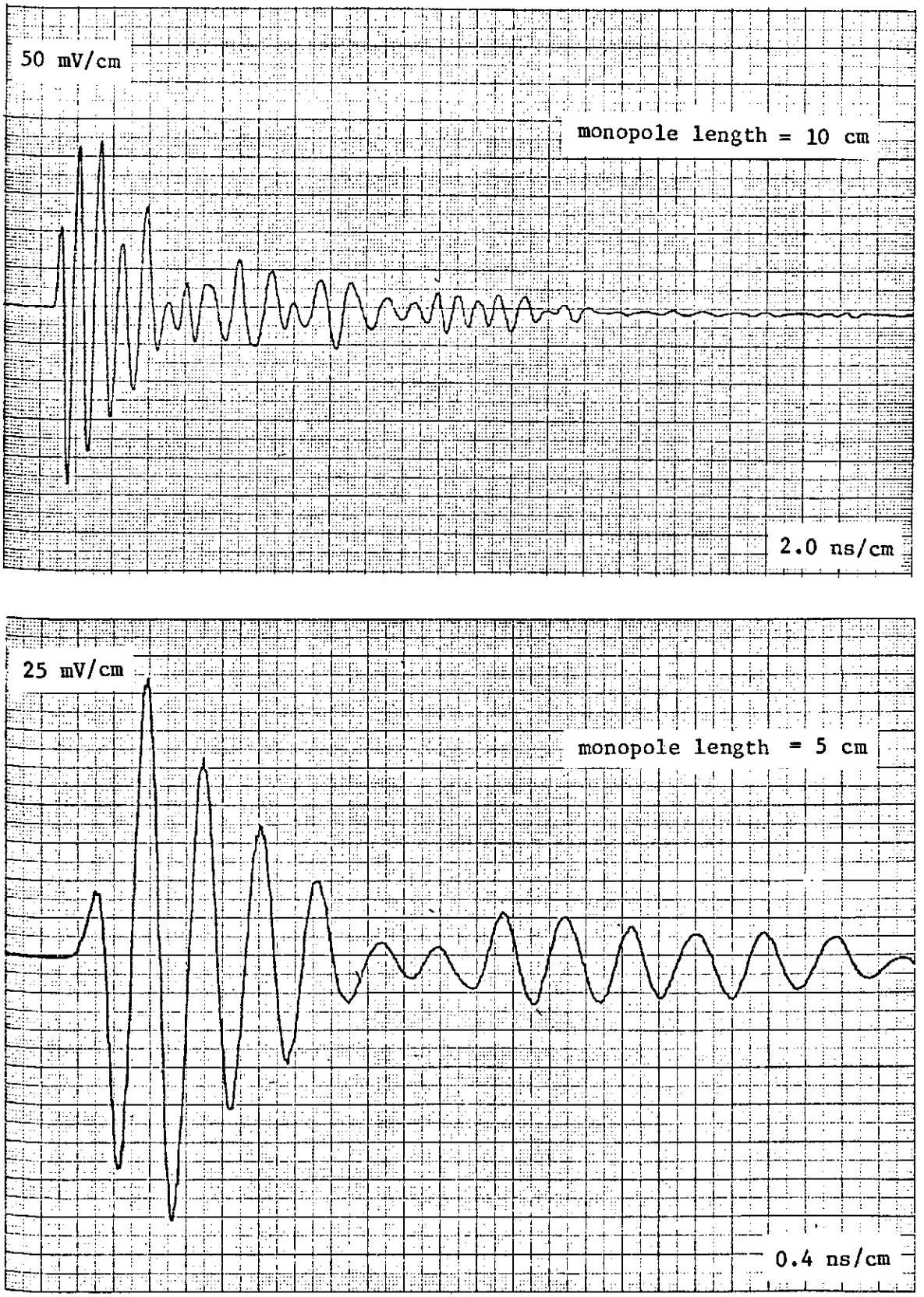

Fig. 6-5 b Comparison of received signals for four antenna lengths. No lossy material present.

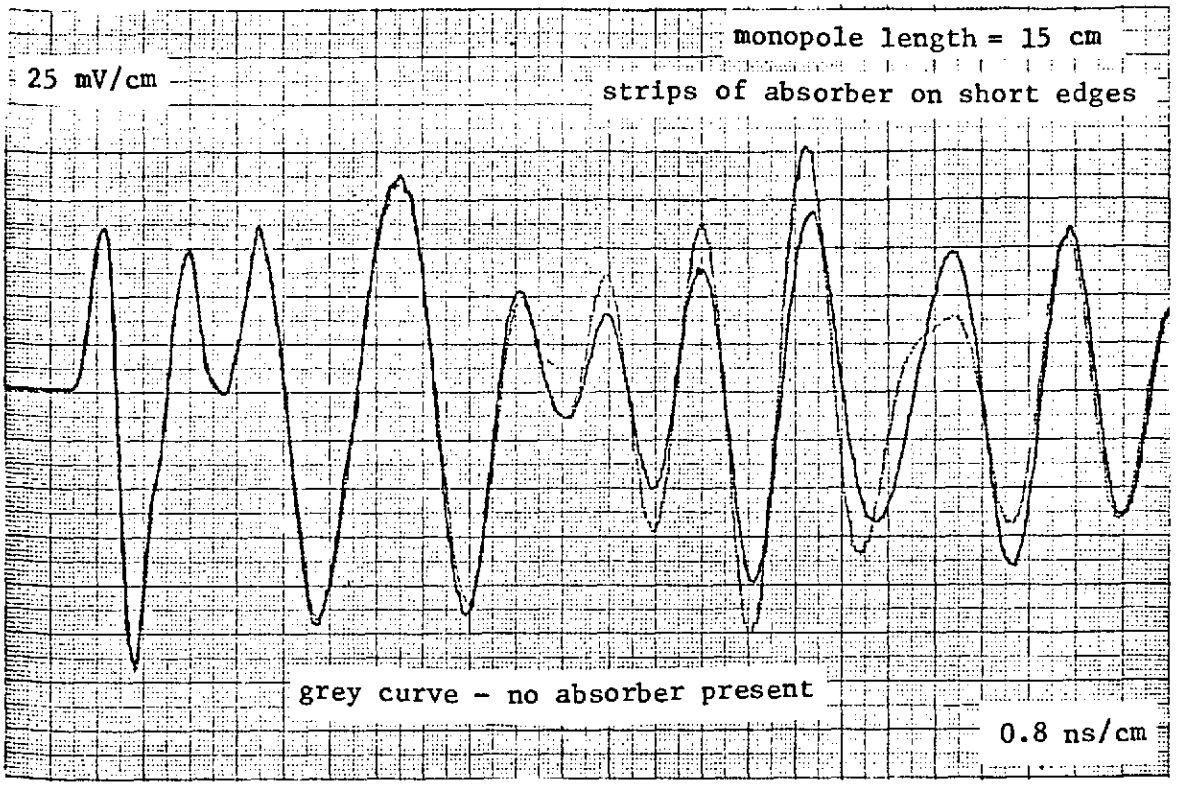

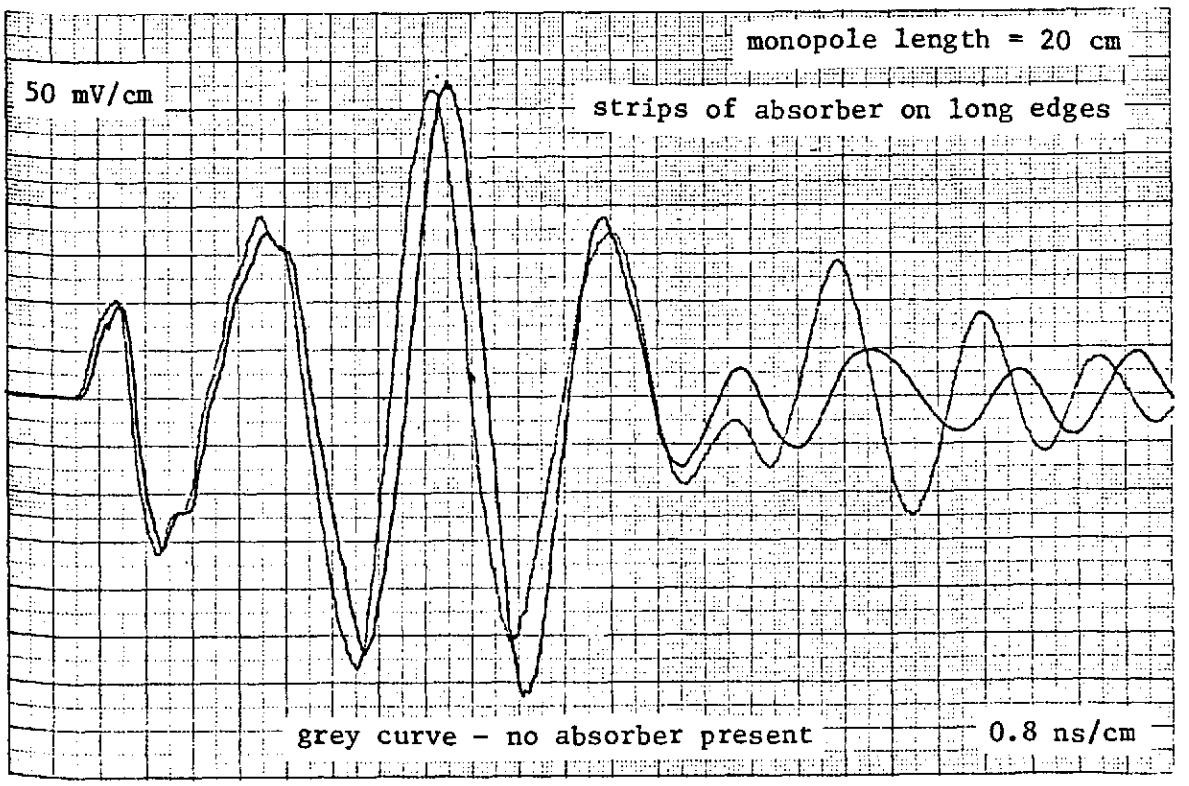

Fig. 6-6 a Effects of lossy material laid on wire grid.

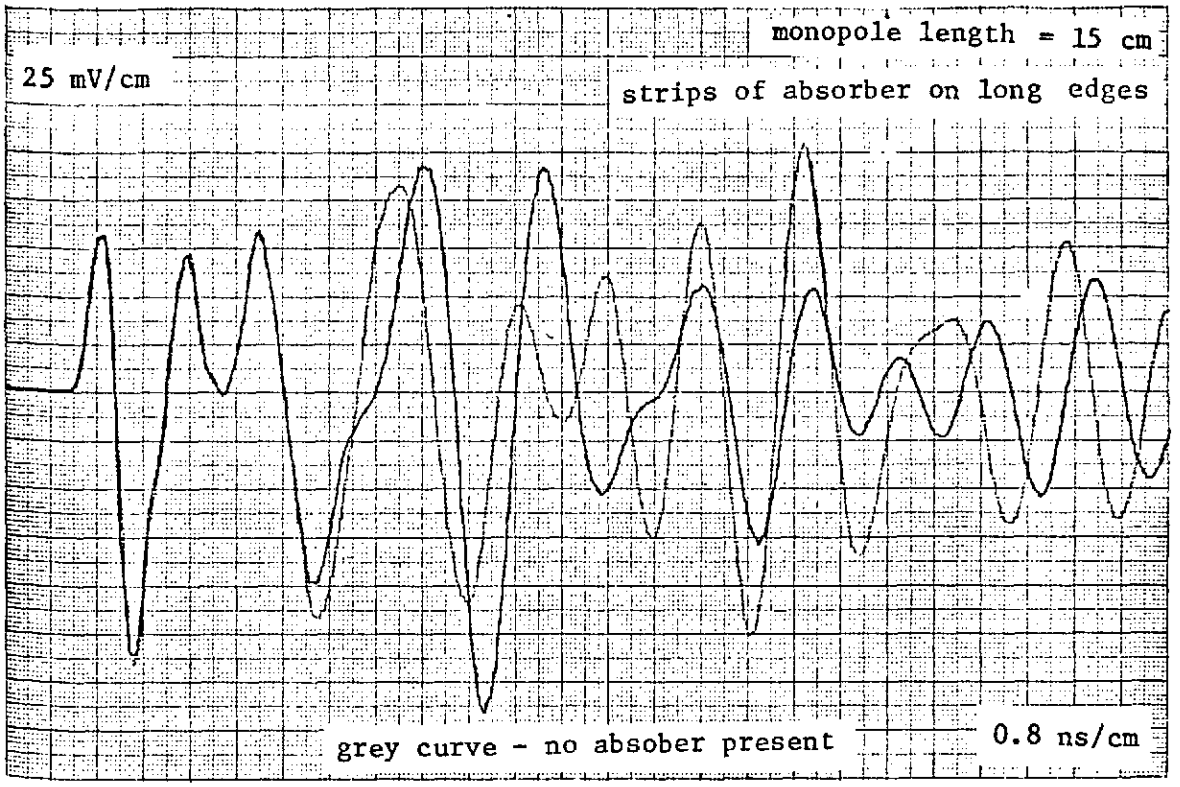

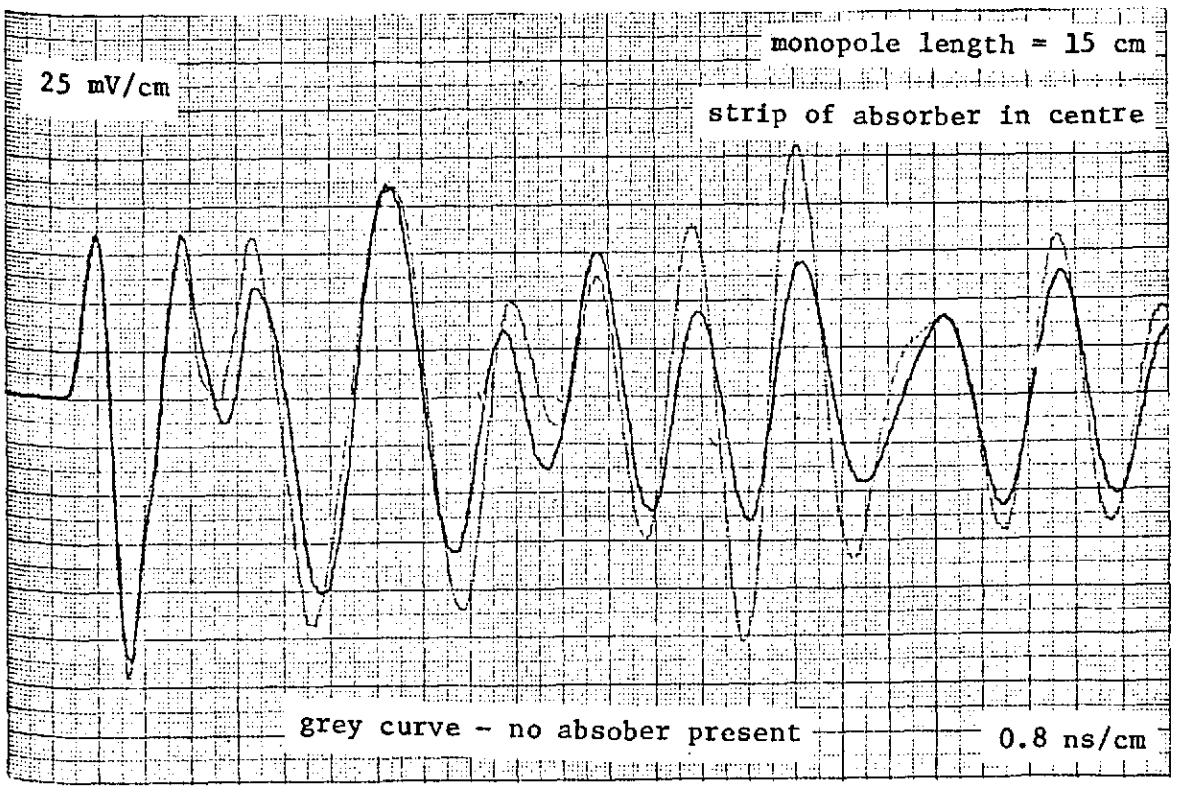

Fig. 6-6 b Effects of lossy material laid on wire grid.

the reflections from the long edges were decreased, the amplitude and the shape of the waveform changed noticeably. The removal of a reflection produces an effect proportional to the previous contribution of the reflection to the received signal; the strength of the reflection can be estimated from the effect.

The last graph of Fig. 6-6 shows the drop in amplitude of the transmitted signal due to a strip of the lossy material laid down accross the grid between the monopoles.

A close examination of the amplitude fluctuations of the long oscillatory tail (region 3 of the received signal, Fig 6-5) reveals beats indicating superposition of two sinusoidal waves. One of them must be due to the antenna, but what is the other one? Probably we have identified a resonance excited on the grid structure, with a resonant frequency determined by the grid spacing "a" through $f_g = c/4a$; it is this grid oscillation which beats with the antenna oscillations.

If the antenna oscillation of frequency f_a beats with the grid oscillation of frequency f_g, a modulated carrier wave with a carrier frequency $f_c = \frac{1}{2}(f_a+f_g)$ and with a modulation frequency $f_m = \frac{1}{2}(f_a-f_g)$, is produced. Since the grid spacing is 0.2 m, then the assumption that this is a quarter wavelength gives a grid frequency of 375 MHz. The resulting carrier and modulation frequencies are compared with the measured values in the table below.

ℓ_a	f_a	f_c	f_m	$T_c = \frac{1}{f_c}$	$T_m = \frac{1}{f_m}$	T_c measured	T_m measured
cm	MHz	MHz	MHz	ns	ns	ns	ns
20	375	375	0	2.667	∞	2.4	-
15	500	437.5	62.5	2.286	16.0	1.9	15
10	750	562.5	187.5	1.778	5.333	1.6	7
5	1500	937.5	562.5	1.067	1.778	0.8	?

The measured values of T_c and T_m agree reasonably well with the theoretical ones.

The grid resonance can also be isolated through the use of a lossy material. A large square hat (23 x 23 x 2cm for the two longer monopoles, and 15 x 15 x 2cm for the two shorter ones) made of Eccosorb LS 22 was placed on the top end of each antenna; their purpose was to damp out the antenna oscillations. The measured received signals are shown in Figure 6-7. The initial pulse build-up is followed by a low frequency oscillation independent of the antenna length. The value of the frequency indicates that the oscillation is the grid resonance. The measured periods of the

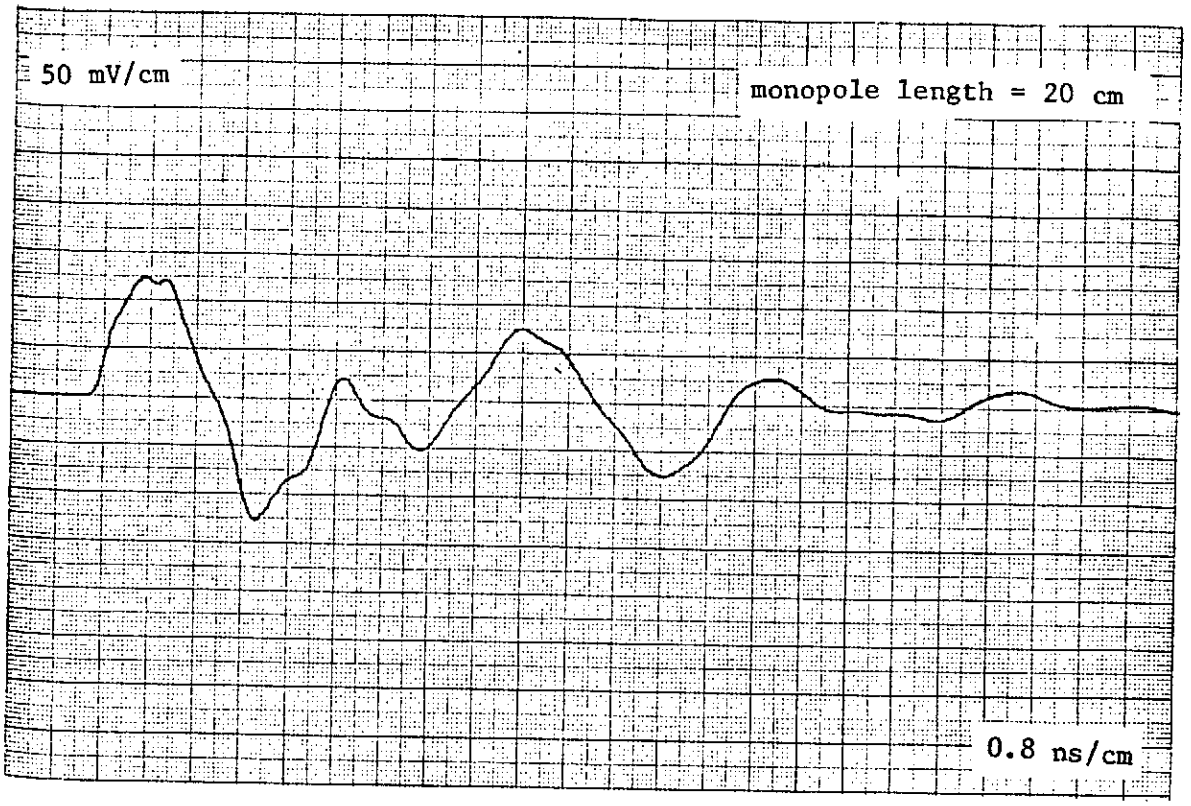

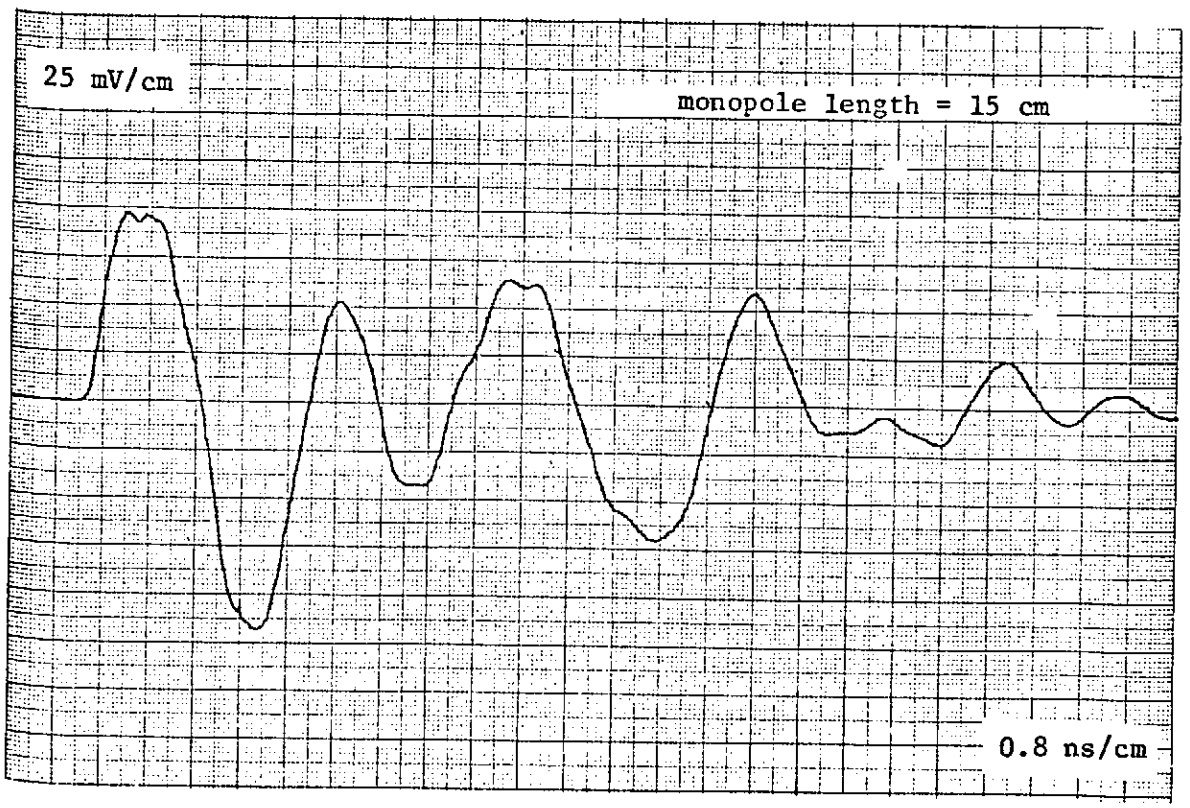

Fig. 6-7 a Signals received by antennas with lossy hats.

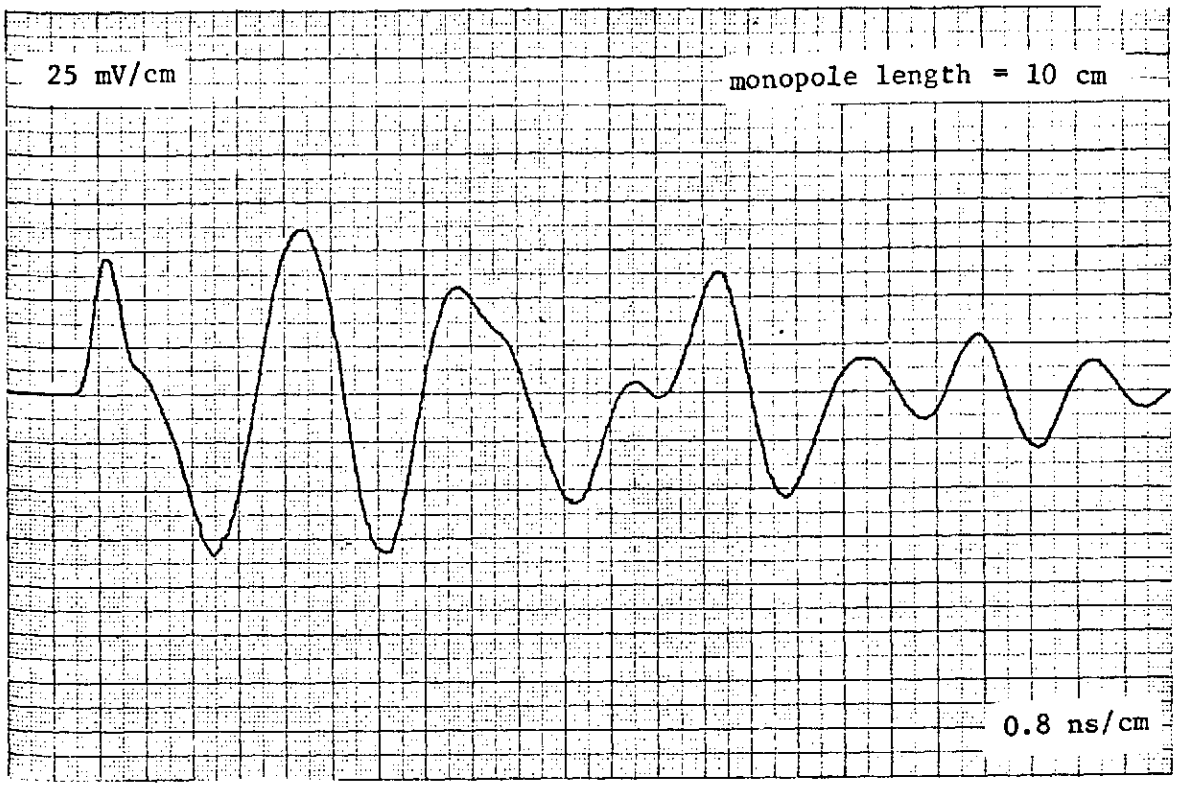

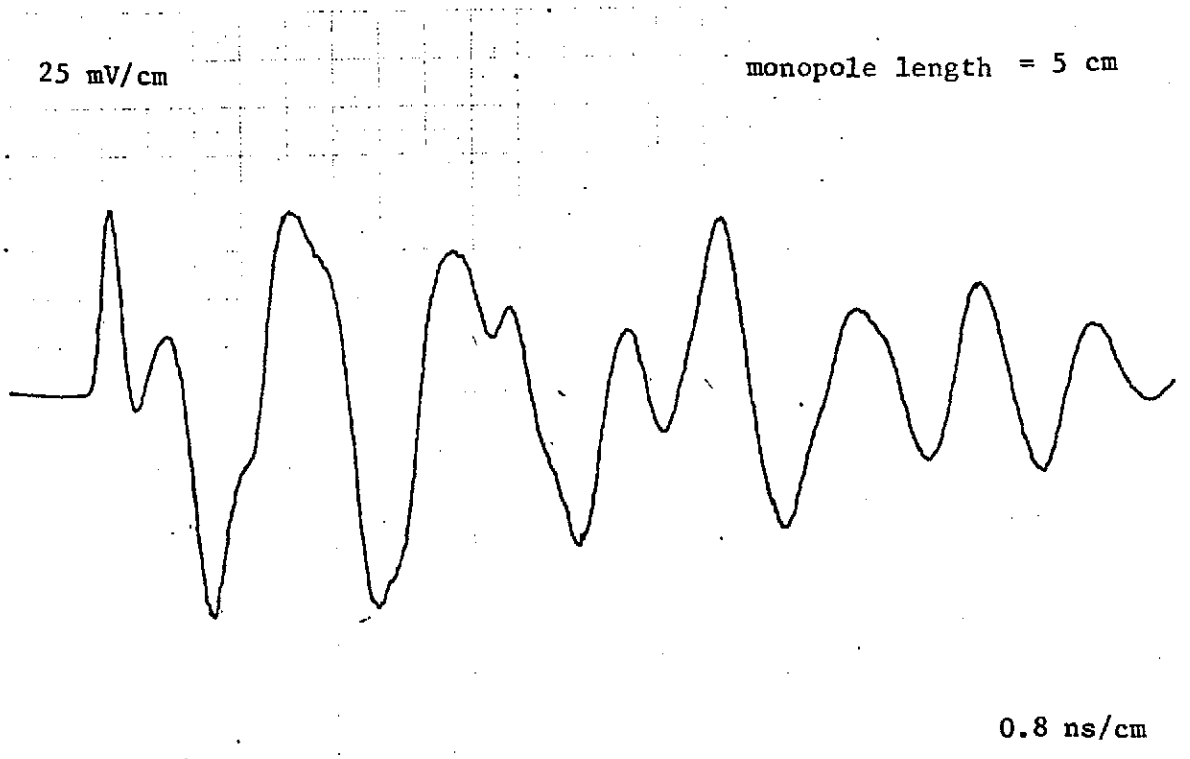

Fig. 6-7 b Signals received by antennas with lossy hats.

oscillation and the corresponding grid frequencies are summarized in the following table.

ℓ_a	T_g (average)	f_g
cm	ns	MHz
20	?	?
15	3.2	312.5
10	2.8	355.4
5	2.7	375.9

Another conclusion that can be drawn from the results in Figure 6-7 is that non-resonant antennas, such as the monopoles with the lossy material hats, can transmit and receive an electromagnetic pulse faithfully. However, if the transmission takes place over a wire grid, a resonance will be excited in the structure and a strong spurious signal will be received.

7. CONCLUSIONS AND RECOMMENDATIONS

K. G. Balmain

7.1 Conclusions

Charge imaging using the scanning electron microscope is a useful procedure for studying charge accumulation, diffusion and decay in a dielectric material, and it is particularly useful for establishing the effective area electrostatically charged by a narrow electron beam. Charge decay is a slow process in general, but is accelerated by continued low-energy electron bombardment and by the application of heat (except for quartz fabric whose charge retention appears to increase with temperature). Partial surface metallization on Teflon causes parallel charged bands to appear near the metallization edge, suggesting the existence of unusually high fields in this region. The use of a television-type dynamic scanning system reveals that the complex charge accumulation patterns (already known to exist) shift slowly as a function of scan area and very rapidly upon the occurrence of a discharge. In general it can be concluded that charge accumulation should be thought of as being highly nonuniform over a nominally smooth and uniform dielectric surface.

Micro-discharges have been identified as a well-defined phenomenon producing current pulses with rise and fall times of the order of a small fraction of a nanosecond. Hundreds of almost-identical discharges can be stimulated in a given small area of Teflon, but the behaviour of Kapton is much more irregular, especially after the first nanosecond of a discharge.

Macro-discharges have peak currents which often scale in a regular way with changes in specimen area. This scaling "law" when extrapolated passes through the estimated region of microdischarges on the one hand and through the very roughly defined spacecraft design region on the other hand. This is the first piece of hard evidence suggesting that the various kinds of surface discharge are just vastly different magnitudes of the same basic phenomenon. This implies that large vacuum systems may be unnecessary for developmental testing of spacecraft insulating materials.

Although discharge pulse peak currents scale upward in a regular way with increasing specimen area, the pulse time durations do not, largely because of the great variability in pulse shape. Nevertheless it can be said that the pulse length does increase with area although not as rapidly as the peak current.

The area dependence described above is clearly associated with the established phenomenon of charge "cleanoff". Apparently, after it is initiated at a point, the discharge propagates very rapidly over an area which is considerably larger than the area covered by arcs or "lighting strokes" which have been seen and photographed. The propagation mechanism and velocity are unknown but the phenomenon could be similar to the very high beam-energy discharges observed by Gross [1958]

Electromagnetic wave attenuation by accumulated charge in a dielectric has been identified experimentally. It is a very weak phenomenon which would have a negligible effect on satellite radio systems employing dielectric antenna covers. Presumably the trapped electrons are able to oscillate in the applied RF field and thus

transfer energy in the form of heat to the host material.

The propagation of a pulse over a complex structure such as a spacecraft would be greatly affected by the structure. In general, multiple reflections and internal resonances would both occur. If an antenna is involved for transmission or pick-up, its own resonances would tend to dominate the measured pulse shape. Therefore discharge detection on a satellite should involve an antenna resonant in a region of high discharge pulse spectral content. A spacecraft antenna electrically damped with a large quantity of lossy material would provide sufficient pulse fidelity to get a good idea of a discharge pulse shape.

7.2 Recommendations

It is possible that imaging of residual charge patterns can be used to identify discharge tracks, in spite of the failure to date in attempts to do this. As yet untried is the idea of polarized-light interaction with a thin surface layer of a field-sensitive fluid such as nitrobenzene or a nematic liquid crystal. The direct imaging of a discharge arc by the use of a photographic emulsion under the specimen could also be be tried.

As for the pulses of discharge current into the specimen pedestal, their fine structure and microwave spectra remain to be measured. Temperature and ultra-violet effects on discharges need to be studied and correlated with the work being done in Europe at ESTEC. Most important of all, the discharge scaling with specimen area needs to be studied carefully, especially as it relates to discharge pulse time

duration and discharge propagation velocity. Pulse measurement capability at the University of Toronto facility should improve greatly within the next few months due to the expected acquisition of a 1000 MHz transient digitizer and a dual-beam 400 MHz oscilloscope

The magnitude of the spacecraft EMI problem could be estimated by the experimental study of pulse penetration into a gridded, skeletal volume resembling a spacecraft. Special attention could be given to the effects of cable harness layout.

Electromagnetic wave absorption by trapped electrons is interesting because it may provide a diagnostic tool for the study of charge accumulation and decay. However the effect is so weak that work on it should not be given a very high priority. A related phenomenon which has not yet been studied is the use of a high level RF signal to stimulate discharge of the material.

In order properly to understand surface arc discharges, their emitted electrons should be studied with regard to spatial distribution and velocity. Direct electron emission on to a phosphor screen should give the spatial distribution. The use of a magnetic field parallel to the specimen surface or an electric field normal to it (via a multi-grid analyzer) should give information about the emitted-electron energies.

Finally, the generation of acoustic waves by a surface arc could be investigated, as a possible diagnostic technique and in order to get further insight into the mechanical stress resulting from a discharge arc. Conversely, mechanical stress stimulation of discharge processes could be investigated.

8. REFERENCES

Adamo, R. C. and J. E. Nanevicz (1976), Spacecraft-charging studies of voltage breakdown processes on spacecraft thermal control mirrors, in Spacecraft Charging by Magnetospheric Plasmas, A. Rosen (Ed.), Progress in Astronautics and Aeronautics, 47, 225-235.

Balmain, K. G. (1973), Charging of spacecraft materials simulated in a scanning electron microscope, Electronics Letters, 9, no. 23, 544-546.

Balmain, K. G., M. Orszag, and P. Kremer (1976), Surface discharges on spacecraft dielectrics in a scanning electron microscope, in Spacecraft Charging by Magnetospheric Plasmas, A. Rosen (Ed.), Progress in Astronautics and Aeronautics, 47, 213-223.

Creswell, R. A., M. M. Perlman, and M. A. Kabayama (1972), The electret properties of a series of corona-charged substituted polyolefins, in Dielectric Properties of Polymers, F. E. Karasz Ed., Plenum Press, N.Y.,295-312.

De Forest, S. E. (1972), Spacecraft charging at synchronous orbit, J. Geophys. Res., 77, 651-659.

Fredricks, R. W., and Scarf, F. L. (1973), Observations of spacecraft charging effects in energetic plasma regions, in Photon and Particle Interactions with Surfaces in Space, Reidel, Dordrecht-Holland, 277-308.

Gross, B. (1957), Irradiation effects in borosilicate glass, Phys. Rev., 107, 368-373.

Gross, B. (1958), Irradiation effects in Plexiglas, J. Polymer Sci., 27, 135-143.

Gross, B., G. M. Sessler and J. E. West (1973), Charge diagnostics for electron-irradiated polymer foils, Appl. Phys. Lett., 22, 315-316.

Hoffmaster, D. K. and J.M. Sellen Jr. (1976), Spacecraft material response to geosynchronous substorm conditions, in Spacecraft Charging by Magnetospheric Plasmas, A. Rosen (Ed.), Progress in Astronautics and Aeronautics, 47, 185-211.

Katon, J. E.,Ed., (1968), Organic Semiconducting Polymers, Marcel Dekker, Inc., N.Y.

Maasland, P.A. (1977), Electromagnetic Wave Attenuation by Spacecraft Dielectrics Irradiated with Electrons, B. A. Sc. Thesis, Div. of Engineering Science, University of Toronto.

Meulenberg, A., Jr. (1976), Evidence for a new discharge mechanism for dielectrics in a plasma, in Spacecraft Charging by Magnetospheric Plasmas, A. Rosen (Ed.), Progress in Astronautics and Aeronautics, 47, 237-246.

O'Dwyer, J. J. (1973), The Theory of Electrical Conduction and Breakdown in Solid Dielectrics, Clarendon Press, Oxford, 286-293.

Reedyk, C. W. (1968), An electret transmitter for the telephone set, in Electrets and Related Charge Storage Phenomena, L. M. Baxt and M. M. Perlman Eds., Electrochemical Society, N.Y., 104-108.

Rosen, A. (1975), Large discharges and arcs on spacecraft, Astronautics and Aeronautics, June 36-44.

Rosen, A. (1976 a), Spacecraft charging: Environment-induced anomalies, J. Spacecraft and Rockets, 13, 129-136.

Rosen, A., Ed. (1976 b), Spacecraft Charging by Magnetospheric Plasmas, Progress in Astronautics and Aeronautics, 47.

Rosen, A. (1976 c), Spacecraft charging by magnetospheric plasmas, IEEE Transactions on Nuclear Science, NS-23, 1762-1768.

Sessler, G. M., and J. E. West (1968), Foil electrets and their use in condenser microphones, in Electrets and Related Charge Storage Phenomena, L. M. Baxt and M. M. Perlman Eds., Electrochemical Society, N.Y., 134-147.

Sessler, G. M., and J. E. West (1970), Charging of polymer foils with monoenergetic low-energy electron beams, Appl. Phys. Lett., 17, 507-508.

Stevens, N. J., R. R. Lovell, and J. V. Gore (1976), Spacecraft-charging investigation for the CTS project, in Spacecraft Charging by Magnetospheric Plasmas, A.Rosen (Ed.), Progress in Astronautics and Aeronautics, 47, 263-275.

Thornton, P. R. (1968), Scanning Electron Microscopy, Chapman and Hall.

Van Turnhout, J. (1975), Thermally Stimulated Discharge of Polymer Electrets, Elsevier Sci. Pub. Co.

Willis, R. F., and D. K. Skinner (1973), Secondary electron emission yield behaviour of polymers, Solid State Communications, 13, 685-688.